Applied Catalysis B: Environmental 132–133 (2013) 266–281

Contents lists available at SciVerse ScienceDirect

Applied Catalysis B: Environmental

journal homepage: www.elsevier.com/locate/apcatb

Mechanistic investigations of the promoting role of Rh on the NSR performance of NO_x storage BaO-based catalysts

Stanislava Andonova[a], Valentina Marchionni[b], Marta Borelli[b], Radka Nedyalkova[a], Luca Lietti[b], Louise Olsson[a,*]

[a] Competence Centre for Catalysis, Chemical Engineering, Chalmers University, 412 96 Gothenburg, Sweden
[b] Politecnico di Milano, P.zza Leonardo Da Vinci, 32, 20133 Milano, Italy

ARTICLE INFO

Article history:
Received 30 May 2012
Received in revised form 2 November 2012
Accepted 12 November 2012
Available online 24 November 2012

Keywords:
NO_x storage/reduction
Pt
Rh
BaO
noble metal
TPD
N_2O decomposition
CO chemisorption

ABSTRACT

To determine the promoting effect of Rh on the overall NO_x storage and reduction (NSR) performance, the studies in the current work were directed toward investigating the storage and release ability over Rh NO_x storage BaO-based catalysts compared to Pt. In terms of the metal surface dispersion and the ability of the noble metals to release oxygen at lower temperatures, the synthesized catalysts were characterized by means of dynamic CO chemisorption (RT) and N_2O dissociation (RT - 773 K). The NO_x storage capacity and the thermal stability of the NO_x adsorbed species formed on the surface were analyzed via NO_x storage tests and temperature programmed desorption (TPD) without and in the presence of CO_2 and H_2O. In addition, experiments with lean and rich cycling were conducted at 473, 573 and 673 K. The results from the N_2O dissociation experiments showed the superior ability of Rh/Al and Rh/Ba/Al catalysts compared to Pt toward O_2 release from the catalytic surface at lower temperatures. In this work, we show that the presence of Rh into the BaO/γ-Al_2O_3 system has a considerable effect on the spill-over process of NO_x to the precious metal, controlling the subsequent desorption of NO_x to occur at lower temperatures in comparison with that of the Pt catalysts. It is suggested a mechanism of NO_x desorption where the lower temperature of O_2 release from the surface of Rh catalysts could leave a significant number of noble metal sites accessible for adsorption. Thus this could facilitate the rate of spill-over of NO_x from the storage site (the surface sites on γ-Al_2O_3 and those on BaO) to the noble metal and their desorption at lower temperatures. The limited NO_x storage ability of the Rh-based BaO/γ-Al_2O_3 catalysts under lean-burn conditions was found to originate from both low NO oxidation activity and NO_x reduction activity, while the main limiting factor for the low NSR performance of the Pt-based catalysts was the limited regeneration ability during rich period.

1. Introduction

The need of better fuel economy and the high standards restricting the NO_x emissions, in particular from diesel-equipped vehicles, have driven the development of highly active and selective catalytic NO_x removal systems operating in oxygen rich conditions. The objective of having efficient catalytic after-treatment converters of NO_x has resulted in the development of a strategy of NO_x storage reduction (NSR) [1,2] based on periodic long lean (in the range of min.) and short rich (for a few seconds) engine combustion phases [3]. Therefore, a requirement of successful NSR catalysts is that the catalyst must be active for both NO oxidation/storage and NO_x reduction.

The NO_x storage and reduction catalytic converters offer high promise for current and future NO_x abatement technology from lean-burning engine exhaust [4,5]. The typical NSR catalytic systems consist of noble metals (Pt, Rh, Pd) for oxidation/reduction purposes, a material with storage potential, e.g., metal oxides like BaO, CaO and γ-alumina as high surface area support. During the lean phase, the NO_x from the engine, mainly in the form of NO, is oxidized to NO_2 on the noble metal sites and stored in the storage component as nitrites and nitrates. When the storage component is saturated, the catalyst is regenerated by switching to fuel-rich conditions. Under rich conditions, the stored NO_x is reduced on the noble metal sites using the excess of CO, HC and H_2 to form N_2, CO_2 and H_2O.

Different experimental [6] and theoretical [7] studies were focused on the effect of the precious metal on the NO_x storage properties and the ability for oxidation and reduction, which determine the overall NSR performance of the exhaust catalysts. It was [6] shown that the Pt as a noble metal component in the NSR

* Corresponding author.
E-mail address: louise.olsson@chalmers.se (L. Olsson).

0926-3373/$ – see front matter © 2012 Elsevier B.V. All rights reserved.
http://dx.doi.org/10.1016/j.apcatb.2012.11.015

system can rapidly convert NO to NO_2 which is subsequently stored predominantly as nitrates, resulting in an improved initial NO_x trapping efficiency and high oxidation activity of the catalysts. However, in former reports [8,9] 1%Pt/17.5%Ba/γ-Al_2O_3 NSR catalyst was studied as a function of the temperature, rich phase duration and reductant concentration. It was found that short regeneration times, low concentrations of reductant and low temperatures resulted in a decrease in NSR catalyst performance over the course of several cycles. This was attributed to incomplete regeneration of the catalyst and the existence of a difference in the rates of NO_x storage and reduction. It was pointed out that readsorption of NO_x released during the rich phase but not reduced quickly enough can be a significant cause of loss of catalyst performance.

In the light of these findings, in recent years a debate has emerged [8] as to the promoting role of the noble metal (Pt and Rh) components over the NO_x storage BaO-based catalyst under lean-burn conditions. Several studies [10–12] were performed in the literature in order to understand the influence of different precious metals (PGM- Pt, Pd, Rh) on the regeneration ability of PM/BaO/γ-Al_2O_3 catalyst. It was found that the type of precious metal affects the NO_x storage properties; in particular for Rh/BaO/Al_2O_3 which shows high reduction ability but relatively low NO_x storage capacity. It was also found that the use of CO as a reducing agent instead of H_2 resulted in a lower NO_x reduction capacity for the Pt/$BaCO_3$/Al_2O_3 catalyst in comparison to the corresponding Rh based sample. Therefore, in addition to Pt, it is suggested that the addition of Rh to the NSR catalyst formulation improves the regeneration and the overall catalyst efficiency. Furthermore, one recent study [13] revealed that the combination of Rh and Pt improves the NO_x reduction efficiency especially when Rh is located on $BaCO_3$ enabling good catalyst regeneration during the fuel rich phase. Moreover, it was found that the bimetallic PtRh-containing catalysts exhibited higher resistivity to SO_2 and the activity decreased negligible upon thermal aging at 1023 K.

An important question regarding the main key aspects of the regeneration process such as the relative rates of regeneration and storage in determining the overall performance of Pt, Rh and Pt/Rh-containing Ba/Al_2O_3 NSR catalysts was discussed in [8]. In this study, the analysis of all products and reactants involved in the regeneration of the catalysts was performed by using realistic regeneration times (ca. 1 s). It was reported that in contrast to Pt catalysts, the rate of regeneration of monometallic Rh/Ba/Al_2O_3 at 523 K and 623 K is sufficient to remove the NO_x stored in the lean phase and the NSR performance strongly depends on the rate of NO_x storage. On the other hand, the amount of NO_x stored on Pt/Ba/Al_2O_3 catalyst at 523 K was found to gradually deteriorate the surface from cycle to cycle until an equilibrium point between the rates of reduction and storage is reached.

Several studies [14–17] suggested that the rate limiting steps controlling the process of NO_x storage and reduction over Pt/Ba/Al_2O_3 strongly depend on the kinetic process of forward spillover of NO_x occurring at the Pt/BaO interface. The higher mobility of surface species between the storage sites and Pt particles was found to enhance the NO_x storage and reduction activity of the catalyst. Based on kinetic modeling studies [18], it has been suggested that the mechanism of release of NO_x from Pt/BaO/Al_2O_3 is spill-over of NO_x to Pt and subsequent desorption of NO_x from Pt. In addition, it was found that the high coverage of oxygen on Pt hinders the spill-over process [18]. Furthermore, one of the recent studies [19] revealed the important role of Pt dispersion on the spillover process. It was pointed out that as the Pt dispersion is increased for a fixed Pt loading, the length of the Pt/BaO interfaces increases, providing additional interface for spillover processes to occur [16,17]. However, the mechanism behind the promoting effect of Rh on the release is still not fully understood.

The objective of this work was to investigate the mechanism of the release of NO_x using different noble metals. This was done by using temperature programmed desorption experiments (NO_2-TPD) on monolithic samples under various atmospheres (Ar, Ar + CO_2, Ar + H_2O): accordingly the effect of CO_2 and water on the NO_x storage and release could be investigated. The effect of the interaction between the noble metals (Pt or Rh) and BaO on the ability to release oxygen from the surface at lower temperatures and the metal surface dispersion were investigated by means of N_2O dissociation and dynamic CO chemisorption. Finally, lean/rich experiments were also performed with flow reactor experiments on the monolith catalysts during which the NO_x uptake/reduction was investigated by alternating phases under lean conditions with the reduction of the released NO_x under rich conditions.

2. Experimental

2.1. Catalyst preparation

Conventional incipient wetness impregnation of γ-Al_2O_3 (171 m^2/g, Sasol Puralox SBa-200) was used for synthesis of Pt/γ-Al_2O_3, Pt/BaO/γ-Al_2O_3, Rh/γ-Al_2O_3 and Rh/BaO/γ-Al_2O_3 catalysts. The samples were synthesized with different noble metal (Pt and Rh) amounts, i.e. 1 wt% Pt and 0.5 wt% Rh, corresponding to identical metal to alumina molar ratio. Pt and Rh supported on γ-Al_2O_3 catalysts were prepared by impregnation of the support material with appropriate concentrations of aqueous solutions of $Pt(NO_3)_2$ (15.46 wt-%, W.C. Heraeus) or $Rh(NO_3)_3$ (9.63 wt-%, W.C. Heraeus). The noble metal precursor solutions were prepared separately and after complete dilution, γ-Al_2O_3 powder (pre-calcined at 1023 K for 2.5 h) was slowly added to the aqueous solutions under constant stirring at room temperature. The slurries were continuously stirred and freeze dried in liquid nitrogen until the water from the suspension was completely removed. After that, the product was ground into a fine powder form and calcined at 773 K for 2 h.

In similar way, the Pt/BaO/γ-Al_2O_3 and Rh/BaO/γ-Al_2O_3 catalysts (the amount of BaO was kept constant at 16 wt% in all samples) were synthesized by the incipient wetness impregnation of the calcined Pt/γ-Al_2O_3 and Rh/γ-Al_2O_3 samples with the aqueous solution of $Ba(NO_3)_2$ (99 wt-%, Sigma-Aldrich). Barium nitrate precursor solution was slowly added under vigorous stirring at room temperature to the pre-prepared solution of Pt(Rh)/γ-Al_2O_3 catalysts dispersed in a certain amount of milli-q water. The mixture was continuously stirred for 1 h and then the slurries were freeze dried and calcined at 873 K for 2 h. Compositions of the prepared catalysts, the surface area and the acronyms used in the current study are presented in Table 1. The calcined powder catalysts were used to coat cordierite monoliths. The monoliths were cut from a commercial honeycomb cordierite structure with a right dimension (length = 20 mm, diameter = 22 mm and cell density of 400 cpsi) and heated to 773 K for 2 h. Then, the procedure consisted of immersing the monoliths into a slurry composed of a liquid phase of equal amounts of distilled water and ethanol and a solid phase of 5 wt% boehmite (Disperal D) and 95 wt% catalyst. The solid in the slurry was 20% w/w. The procedure of the immersing, blowing away the excess slurry, drying (363 K for 2 min) and heating (823 K for 2 min) in air was repeated several times until the monolith was coated with the desired amount of washcoat (∼ 700 mg, corresponding to 20% w/w). Finally, the wash-coated monoliths were calcined at 773 K for 2 h.

2.2. Catalyst characterization

Specific surface area - The total surface area (S_{BET}) of the calcined catalysts preliminary degassed at 473 K for 2 h was determined

Table 1
Surface area (S^{BET}), amount of chemisorbed CO, N_2 produced during N_2O decomposition, Metal Dispersion (MD) and NO_x trapping efficiency of the catalysts.

Catalysts	Noble metal loading (%)	S^{BET} (m^2/g)	CO_{ads}, mol/g_{cat} ($\times10^{-5}$)	$N_{2\ prod.}$, mol/g_{cat} ($\times10^{-5}$)	MD[a] (%)	NO_x trapping efficiency (%)	NO_x trapping efficiency (%) in CO_2	NO_x trapping efficiency (%) in H_2O
γ-Al_2O_3	-	171	-	-	-	7.1	8.2	4.3
Ba/Al	-	131	-	-	-	13.5	14.0	26.1
Pt/Al	1	184	1.7	1.1	21.7	7.8	8.4	4.9
Pt/Ba/Al	1	131	0.9	0.6	11.1	13.7	14.1	27.2
Rh/Al	0.5	181	4.7	3.2	65.4	7.3	7.8	4.1
Rh/Ba/Al	0.5	135	3.2	2.1	42.3	13.9	14.4	25

[a] The MD calculated based on the N_2O dissociation performed at 373 K by assuming that the number of formed N_2 molecules is equal to the number of surface Me sites.

using the nitrogen adsorption data from the relative equilibrium pressure interval of 0.03–0.3 P/P_0 according to the standard BET procedure using a Micromeritics ASAP 2010 instrument.

N_2O Dissociation with powder catalysts–The experimental set-up used for the N_2O dissociation measurements comprises a vertical quartz tube reactor mounted in an electric furnace, part of the assembly of the heat-flux Differential Scanning Calorimetry (Setaram Sensys DSC) instrument. The gas flow into the reactor was controlled by using a system of mass flow Bronkhorst controllers. Prior to each measurement, the catalyst (approximately 0.1 g of powder sample placed on the sintered bed of the quartz tube) was first subjected to degreening with a mixture of 5% O_2 for 3 h. Then after flushing with Ar, the samples were pre-reduced for 30 min in 1% H_2 at 823 K and the temperature was then decreased to the target reaction temperature. The catalysts were exposed to 200 ppm N_2O for 1 h at different temperatures (298 – 773 K). Argon was used as an inert balance and the total flow was 20 ml min^{-1}. The effluent from the reactor was monitored using a Hiden HPR 20 quadrupole mass spectrometer (MS) equipped with a capillary probe connected directly to the exit of the reactor. The analysis of the reaction products and the unreacted N_2O were monitored by recording the MS signals with mass to charge ratio (m/e) equal to 28, 32 and 44 in pressure vs. time mode. The noble metal dispersion (Pt and Rh) is determined by integrating the N_2 (m/e 28) signal during the N_2O exposure step at 373 K after subtracting the contribution which originates from the cracking of N_2O in the MS. The number of formed N_2 molecules is considered to be equal to the number of surface noble metal sites [20].

To evaluate the surface metal dispersion (MD) of the catalysts, the N_2 from the N_2O dissociation at 373 K was used to determine the volume of N_2 produced during the dissociation process. The MD (%) was estimated according to Eq. (1), as follows:

$$MD(\%) = \frac{V_m * A_w * 10^4}{W\% * S_f} \quad (1)$$

Where, V_m is monolayer volume (mol N_2 g^{-1} sample); A_w is the metallic atomic weight (g metal mol^{-1}); W% is metal loading and S_f is the stoichiometric factor assumed ~1 in the N_2O decomposition experiments (i.e. the number of formed N_2 molecules is equal to the number of surface metal sites [20,23]).

Dynamic CO chemisorption with powder catalysts–The experimental set-up given above was also used to measure the amount of irreversibly chemisorbed CO on the surface according to the Holmgren and Andersson's method [21]. In these experiments, after the degreening and reduction step, which were described above, the catalysts were exposed to 200 ppm CO for 1 h in two steps at room temperature (298 K) with flushing with Ar between the first and second exposure step. The amount of chemisorbed CO was determined as a difference between the first and second CO concentration profiles superimposed in the same time scale, by assuming an adsorption of 0.7 CO molecules per surface Me atom [22]. Next, after the second CO exposure step, the sample was flushed with Ar for 20 min and subsequently, TPD experiments were carried out. Evolved species during the desorption process were monitored by recording the MS signals with mass to charge ratio (m/e) equal to 2, 28 and 44. A linear temperature ramp within 298–823 K was used during the TPD experiments with a ramp speed of 20 K min^{-1}.

NO_x storage reduction measurements with monolith catalysts - The experimental set-up used for the NO_x storage tests, TPD and the lean and rich cycling experiments on the monolith catalysts has been described in detail elsewhere [24]. The monolith catalyst was inserted in the middle of the heated zone of a horizontal quartz tube reactor, which was equipped with an insulated heating wire controlled by Eurotherm temperature-controller. The temperature was measured with a thermocouple positioned about 10 mm in front of the monolith and a second thermocouple placed in the center of the monolith. The total gas flow rate was held constant at 3500 ml min^{-1} and controlled by a system of mass flow Bronkhorst controllers. The water in the form of steam was introduced into the reactor by using a controlled evaporation and mixing Bronkhorst system. All lines were heated and maintained at temperatures above 423 K to prevent water condensation. Approximately 700 mg catalyst washcoated on the monolith was used in each experiment yielding a space velocity of 30,300 h^{-1}, based on monolith volume (or about 300,000 h^{-1} based on washcoat volume). The monoliths were wrapped with quartz wool to ensure that no gas slipped around the sample. The outlet gas composition from the reactor flow was monitored and analyzed on-line with respect to NO, NO_2, N_2O, NH_3, CO, CO_2 and H_2O content by using MKS MultiGas 2030 HS FTIR spectrometer.

To maintain a constant catalytic behavior over the course of the study, the catalysts were degreened by increasing the temperature to 823 K in Ar; then the samples were cleaned/conditioned with 1% H_2 for 30 min, flushed with Ar for 5 min and then the catalysts were treated with a gas mixture of 500 ppm NO + 5% O_2 + 5% CO_2 + 5% H_2O and balancing amounts of Ar for 3 h. The reactor temperature was then cooled to the target test reaction temperature in the presence of Ar.

The following experiments were carried out:

a) NO_x storage tests and TPD in/without the presence of H_2O or CO_2 - Prior each experiment, the catalysts were heated to 773 K in Ar and then 1% H_2 was introduced for 15 min. After flushing in Ar, the samples were pre-oxidized in 5% O_2 for 15 min, and finally the reactor temperature was cooled down in Ar to 423 K and the NO_x storage experiments were then performed. The catalysts were exposed to 500 ppm NO_2 for 1 h and after flushing with Ar for 30 min, the temperature was raised to 773 K with a ramp speed of 10 K min^{-1}. In addition, in order to investigate the effect of H_2O and CO_2, 5% of each was introduced individually during the NO_x uptake and during the desorption analysis. The outlet NO_x concentration was monitored as a function of time and then converted to the cumulative NO_x trapped as a percentage of the NO_2 fed. In this way, the NO_x trapping efficiency was calculated as a ratio of the total NO_x stored to the total amount of NO_2 fed during the uptake period.

b) Lean and rich cycling experiments - To evaluate the NSR performance of the catalyst, the experiments of storage/reduction cycles were performed in the flow reactor system described above.

The monolith catalyst sample mounted in the center of the horizontal quartz tube reactor was pre-treated using the identical procedure given above consisting of reduction in 1% H_2, flushing in Ar and oxidation in 5% O_2 at 773 K. Then, the reactor temperature was decreased to the target test reaction temperature and the lean and rich cycling experiments were conducted. The measurements were carried out at 473, 573 and 673 K with constant total flow rate of 3500 ml min^{-1} and catalyst mass of ~700 mg, giving a space velocity of 30,300 h^{-1}, based on monolith volume (or about 300,000 h^{-1} based on washcoat volume). NO was continuously fed during lean and rich cycles. The cycles consisted of 4 min of storage (lean period) and 1 min of release/reduction (rich period). For this purpose two reaction mixtures were alternated in a predefined sequence of ten cycles. During the lean period the inlet gas mixture consisted of 10% O_2, 500 ppm NO, 5% CO_2, 5% H_2O and a balance of Ar. After 4 min, the gas composition was switched to abundant in H_2 for 1 min (gas composition in the rich period: 500 ppm NO + 1% H_2 + 5% CO_2 + 5% H_2O and a balance of Ar).

To evaluate the NSR performance of the catalysts, the outlet concentration curves during the lean and rich cycling experiments were used to determine the NO oxidation activity, NO_x trapping/removal efficiency and N_2/NH_3 selectivity [25]. The results were obtained over the cycles after the system had reached a cyclic steady-state. NO oxidation activities of the catalysts were determined by calculating the NO conversion, according to Eq. (2) by:

$$X_{NO} = \frac{\left[NO_2^{out}\right]}{\left[NO_2^{out}\right] + [NO^{out}]} \times 100 \quad (2)$$

The total NO_x stored during the lean period was calculated by using Eq. (3):

$$[NO_x^{stored}] = (NO^{in})_{tL} - (NO_x^{out})_{tL} \quad (3)$$

$(NO^{in})_L$ is the total integrated NO concentration at the reactor inlet during the lean period, $(NO_x^{out})_L$ is the total integrated NO_x concentration at the reactor outlet during the lean period and t_L is the length of the lean period (min).

The outlet NO_x concentration was monitored as a function of time and then converted to the NO_x trapped as a percentage of the NO fed, according to Eq. (4):

$$NO_{xTrappingEfficiency} = \frac{NO_L^{in} - NO_{x,L}^{out}}{NO_L^{in}} \times 100 \quad (4)$$

The NO_x removal efficiency was calculated from the evolution of NO_x concentration (Eq. (5) with time during both lean and rich cycles, as:

$$NO_{xRemovalEfficiency} = \frac{NO_{L+R}^{in} - NO_{x,L+R}^{out}}{NO_{L+R}^{in}} \times 100 \quad (5)$$

NO_{L+R}^{in} and $NO_{x,L+R}^{out}$ are the total integrated inlet NO and outlet NO_x concentration during the lean and rich period.

The corresponding selectivity to NH_3 was calculated as the amount of NH_3 at the reactor outlet (during the rich period and the first part of the subsequent lean period) related to the total amount of N-containing products (Eq. (6)):

$$S_{NH_3} = \frac{NH_3^{out}}{NO_{x,L}^{stored} + NO_R^{in} - NO_{x,R}^{out}} \times 100 \quad (6)$$

NH_3^{out}, $NO_{x,L}^{stored}$, NO_R^{in} and $NO_{x,R}^{out}$ are the total integrated outlet NH_3 concentration during the rich and lean periods, the NO_x stored during lean period, the total integrated inlet NO and outlet NO_x concentration during the rich period, respectively.

Selectivity to N_2 was calculated based on the nitrogen balance during rich period expressed, according to Eqs. (7) and (8):

$$N_2^{out} = \frac{1}{2}\left[NO_x^{stored} + (NO^{in})_R - NH_3^{out} - (NO_x^{out})_R\right] - N_2O^{out} \quad (7)$$

$$S_{N_2} = \frac{[2N_2^{out}]}{[NH_3^{out}] + [2N_2^{out}] + [2N_2O^{out}]} \quad (8)$$

3. Results and discussion

3.1. Noble metal surface dispersion

The measurements based on the method of dynamic CO chemisorption [21] were performed for both binary Pt/Al, Rh/Al and ternary Pt/Ba/Al and Rh/Ba/Al mixed systems. Fig. 1A and B presents the results corresponding to Pt/Ba/Al and Rh/Ba/Al catalysts. The insets of Fig. 1C and D show the amount of the irreversibly chemisorbed CO on the surface metal (Pt and Rh) sites determined as a difference between the first and second CO concentration profiles superimposed in the same time scale. The results for all catalysts are also summarized in Table 1. From both Fig. 1A and B, it can be seen that the CO signal during the first exposure step is greatly delayed in comparison to the second exposure cycle until the systems reach a steady-state level. It is apparent that during the first exposure step, CO is chemisorbed on reduced noble metals until all surface sites are saturated with CO. The intensity of the second CO signal starts to increase immediately when the CO exposure is initiated, indicating that the adsorption of CO during the second step forces only weakly bounded CO molecules to adsorb on the surface.

Regarding the amount of the irreversibly chemisorbed CO on the catalysts, there are large differences between the samples, particularly in the case of the Rh/Al and Rh/Ba/Al system in comparison to that for Pt catalysts (Table 1). It should be mentioned that the CO chemisorption is often used to determine the metal dispersion; the adsorption stoichiometry for Rh catalysts varies between 1 and 2 depending on particle size [26,27]. In addition, the results from TPD analysis performed in our study after the two steps of CO chemisorption, presented in Fig. 1 showed that the Rh containing catalyst is characterized with significantly higher amounts of desorption products mostly in the form of CO_2 and CO with minor contribution of H_2 during the temperature ramp in comparison with the Pt catalyst. The origin of these desorption products was discussed in different former studies. Accordingly, it is suggested [28–30] that the source of the desorbed hydrogen is due to the H_2 accumulation on the catalyst surface during the pre-reduction of the samples and during the cooling step. Along similar lines, the CO and CO_2 desorption was found [11,31] to originate mostly from the accumulation of CO on the catalytic surface in the form of carbonyls and carbonates produced by the reactions of CO with residual traces of O_2 and water. The presence of water (or surface hydroxyls) may also explain the H_2 formation by the reaction with CO according to the water gas shift reaction (WGSR) by Eq. (9):

$$CO + H_2O \leftrightarrow CO_2 + H_2 \quad (9)$$

In the light of these observations, it is suggested that not only the higher metal dispersion but also the enhanced formation of carbonates due to residual oxygen in the sample would increase the CO storage capacity, especially in the case of Rh/Al and Rh/Ba/Al catalysts. Thus, it was concluded that the carbonate formation and accumulation phenomena occurring on the surface estimated by the method of dynamic CO chemisorption might contribute to the Rh dispersion.

Therefore, further information about the metal surface dispersion of Rh and Pt catalysts was obtained by analyzing the results from N_2O dissociation performed on the catalysts at 373 K. In Fig. 2A

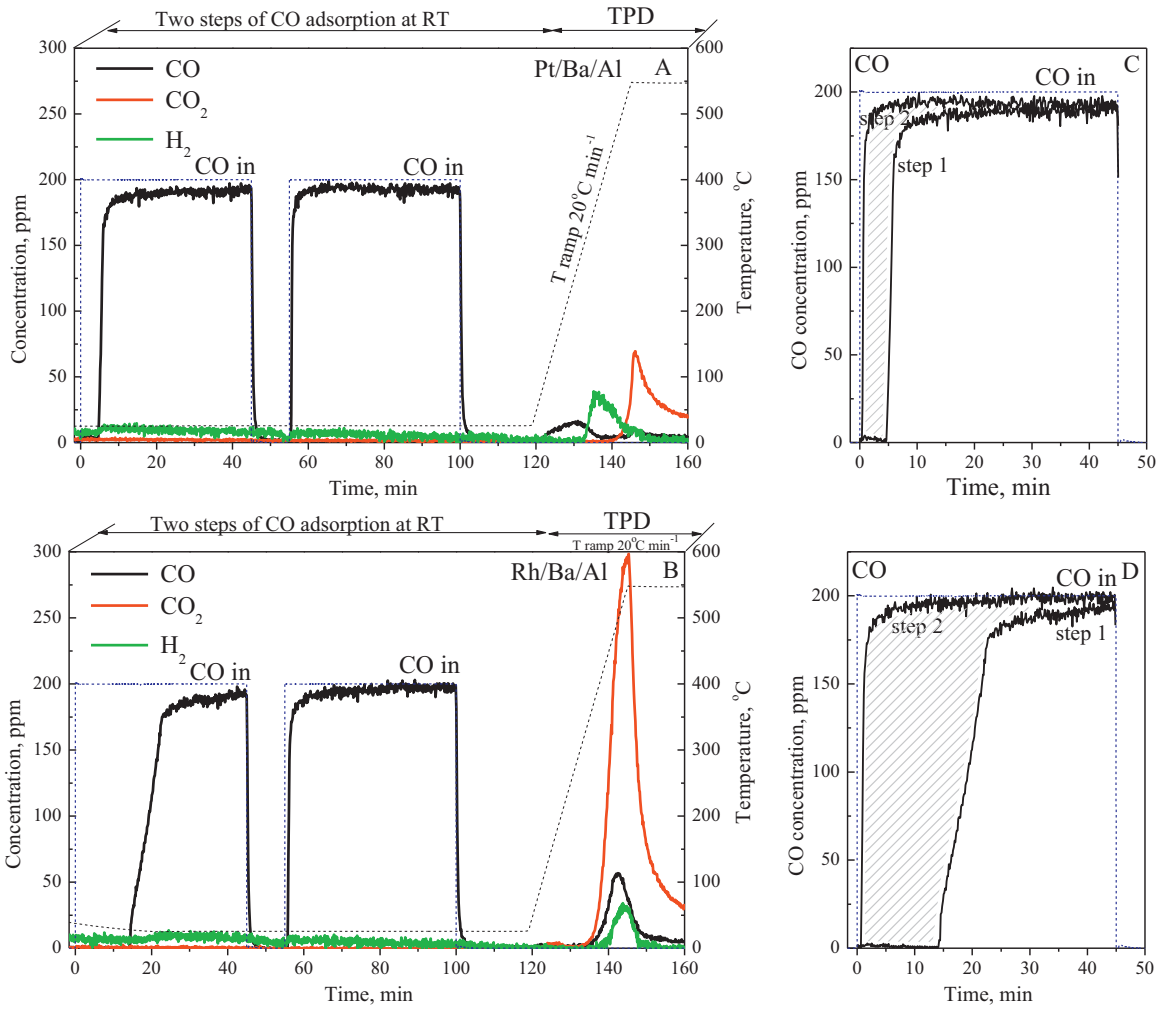

Fig. 1. Dynamic CO chemisorption at RT and TPD of the Pt/Ba/Al (A) and Rh/Ba/Al (B) catalysts that were initially saturated with 200 ppm CO/Ar for 1 h in two steps. Insets (C and D) present the concentration of CO during the first and second CO exposure steps superimposed on the same time scale for both catalysts.

and B the results for Pt/Al and Pt/Ba/Al sample are shown, whereas Fig. 3A and B presents the data for Rh/Al and Rh/Ba/Al catalysts, respectively. From both Figs. 2 and 3, it can be seen that N_2O dissociation process starts to occur immediately when the N_2O exposure is initiated with the formation of N_2 until the steady state was reached. The observed concentration profiles are in a good agreement with the proposed [32–34] general mechanism of catalytic N_2O decomposition at low temperatures which yields N_2(g) and O(ads), with the latter remaining adsorbed on the surface. It can be also seen that the N_2 production at the maximum N_2O conversion continues until the saturation point where N_2O signal start to increase simultaneously when the N_2 feature attenuates. The decomposition reaction results in the formation of N_2 without any O_2 release in the gas phase. Apparently, the surface sites on the noble metal are progressively filled by chemisorbed oxygen atoms starting at the front of the bed and proceeding along it in chromatographic fashion.

The metal dispersion MD (Table 1) was determined by assuming that the number of formed N_2 molecules is equal to the number of surface metal sites (or that the oxidation process has resulted to the formation of almost complete oxygen monolayer). The total amount of N_2 produced during the N_2O exposure was calculated by integrating the signal of N_2 until the saturation point where N_2O reached the value corresponding to minimum conversion. It should be mentioned that it is possible that Rh oxides are formed during N_2O dissociation, with a stoichiometry between O and Rh that is larger than 1. This would result in an overestimation of the dispersion of Rh containing samples, in the same way has for the CO chemisorption where residual oxygen might be left on the surface.

Comparison of the results regarding the metal dispersion of the Pt and Rh catalysts determined by the method of N_2O dissociation can be seen in Table 1. It is readily visible that the catalysts can be ranked in terms of increasing metal dispersion as follows: Pt/Ba/Al < Pt/Al < Rh/Ba/Al < Rh/Al. The values corresponding to Rh/Al and Rh/Ba/Al catalysts are near to 65% and 42%, respectively, while those for Pt samples tend to decrease to 21% for Pt/Al and about 11% for Pt/Ba/Al, respectively. If assuming 0.7 CO per noble metal atom, which is suggested for Pt, the dispersions from the CO chemisorption are 68, 46, 24 and 13%, respectively. Thus, very similar dispersions were obtained. Moreover, it can be seen that the most significant loss of the dispersion has occurred for the Pt and Rh samples containing the BaO NO_x storage component. This effect is especially visible for Pt/Ba/Al catalyst in comparison with that of Rh/Ba/Al sample. In fact, the effect of the presence of the storage BaO material on the Pt metal dispersion has been already discussed in the literature [6,18] and explained by the physical cover of Pt caused by the BaO particles.

In addition, it can be also seen, especially in the case of Rh/Ba/Al catalyst at 373 K (Fig. 3B), that the deviation of the N_2O and N_2 signals is also accompanied by O_2 production (~ 40 ppm) although the temperature was maintained constant during the whole experiment. Moreover, the appearance of O_2 coincides with an increase

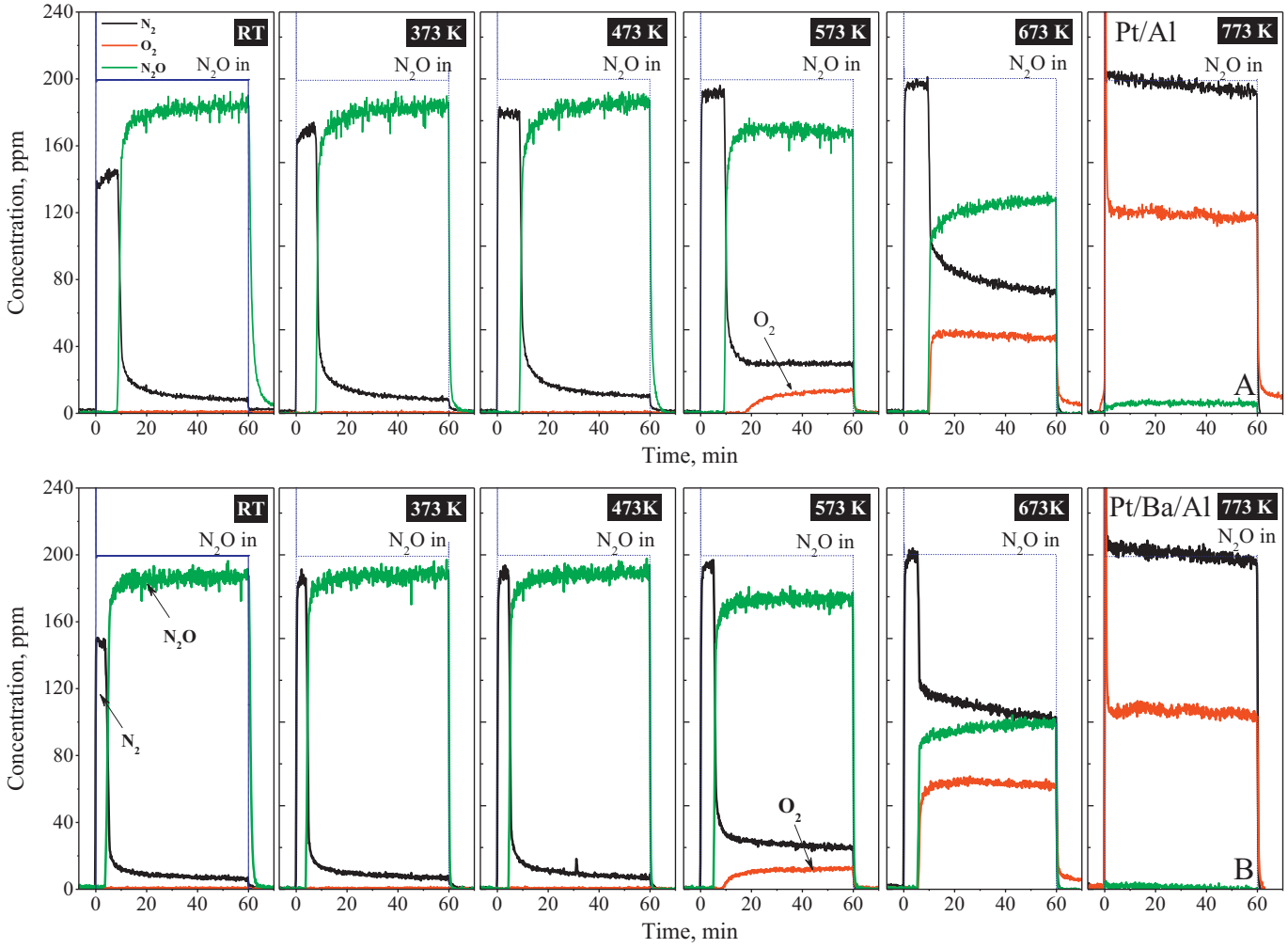

Fig. 2. Dissociative N_2O adsorption over Pt/Al (A) and Pt/Ba/Al (B) catalysts at different temperatures (RT, 373–773 K). Prior to each measurement, the catalyst (~0.1 g) was first subjected to degreening with a mixture of 5% O_2 for 3 h. Then after flushing with Ar and reduction in 1% H_2 at 823 K, 30 min, the catalysts were exposed to 200 ppm N_2O for 1 h at different temperatures.

in N_2O conversion and N_2 production. In former studies [35,36] investigating the mechanism of O_2 release from Rh catalysts, it is suggested that O_2 formation comes from the recombination of two adsorbed oxygen through a Langmuir-Hinshelwood mechanism at high temperature and from reaction-assisted desorption of O_2 at low temperature. The observed oxygen signal in the case of Rh/Ba/Al catalyst suggests that the surface coverage of oxygen has reached a critical level and the kinetic energy of the N_2O molecules may be sufficient to accelerate some recombination and release of O_2 that would otherwise require higher temperatures. In contrast, such a situation is not valid for Pt/Al and Pt/Ba/Al samples where the oxygen accumulation has resulted in a minimum in N_2O conversion and N_2 production (~10 ppm) until the end of the exposure period. It is evident from Fig. 2A and B at 373 K that the reaction of N_2O decomposition to N_2 occurs without any $O_{2(g)}$ formation which coincides with a decrease in N_2O conversion beyond the saturation point.

3.2. N_2O Dissociation

Further insight regarding the oxygen blocking of the Pt and Rh catalysts and their ability to release O_2 from the surface was obtained by focusing on the results from the series of N_2O (200 ppm) dissociation experiments performed at different temperatures. The evolution of N_2O and the reaction products during catalytic N_2O decomposition over the catalysts and the temperature of O_2 release were studied as a function of the reaction temperature (298–773 K). In Fig. 2A and B the catalytic performance of Pt/Al and Pt/Ba/Al are presented while in Fig. 3A and B are given the results for Rh/Al and Rh/Ba/Al samples, respectively.

It can be clearly seen that at all temperatures the dissociation reaction is immediately observed when the N_2O exposure is initiated. The overall reaction has resulted mainly in the production of N_2 accompanied with the formation of small quantities of O_2 whose distribution depends on the reaction temperature and on the catalyst. Comparison of the results reveals that the temperature at which steady state N_2O conversion of ~100% is achieved is significantly lower for Rh catalysts (at about 473 K) than that observed for Pt/Al and Pt/Ba/Al samples (at about 773 K). Moreover, in contrast to the Pt catalysts, after increasing temperature in the range of 373–473 K, significant alteration in the N_2O conversion and N_2 production is observed. The later is also accompanied with the appearance of O_2 signal at 373 K for Rh/Ba/Al catalyst and at 473 K for Rh/Al. It is interesting to notice for Rh/Al catalyst that the time corresponding to maximum production of N_2 and complete N_2O dissociation at all temperatures above 373 K is approximately 50% longer than that at lower temperatures. A possible explanation for that is the slow formation of Rh oxide species, which have different reactivity. The formed rhodium oxides might have different stoichiometry at low and high temperatures, which can explain the

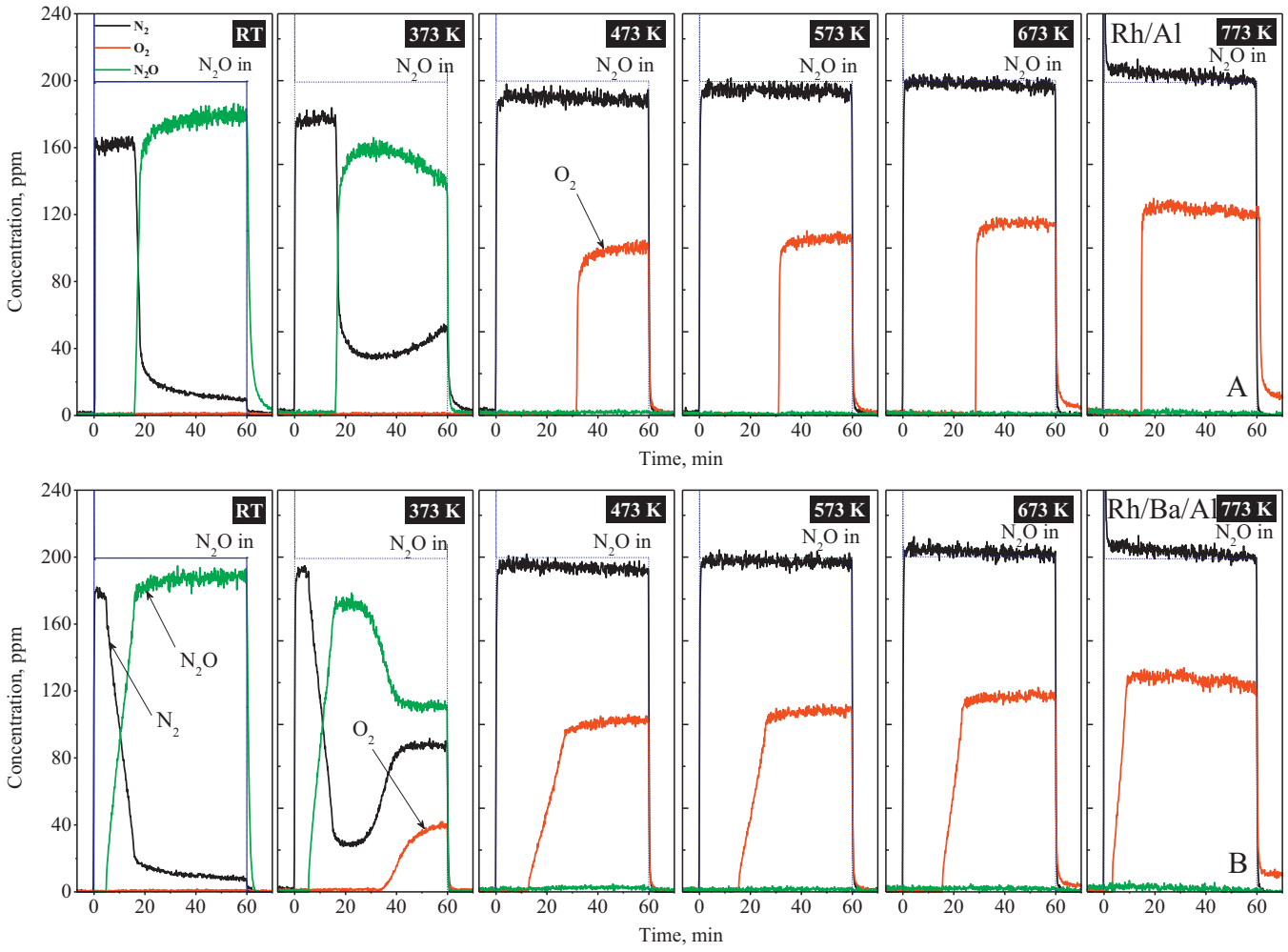

Fig. 3. Dissociative N_2O Adsorption over Rh/Al (A) and Rh/Ba/Al (B) catalysts at different temperatures (RT, 373–773 K). Prior to each measurement, the catalyst (~0.1 g) was first subjected to degreening with a mixture of 5% O_2 for 3 h. Then after flushing with Ar and reduction in 1% H_2 at 823 K, 30 min, the catalysts were exposed to 200 ppm N_2O for 1 h at different temperatures.

observed features. However, in any case, the appearance of O_2 in the gas phase clearly shows the point where the noble metal active sites were fully saturated by oxygen on the surface. Thus, once O_2 started being released from the surface it facilitates the recycling of the active sites and accelerates the decomposition process. Such a situation is not valid for Pt catalysts as can be seen from Fig. 2A and B where no O_2 signal was detected at temperatures below 573 K. According to Tanaka et al. [36] oxygen desorbs at higher temperature during O_2 TPD experiments compared to N_2O dissociation experiments. This was explained by the reaction- assisted desorption. Moreover, it can be suggested that that the oxygen release is the rate-limiting step in the reaction of N_2O dissociation.

In the light of these results, it can be argued that Rh catalysts seem to be more active than Pt in the ability to release O_2 from the surface at lower temperatures, maintaining Rh in metal state. In a former study [37], it was found that the nature and structure of metal particles have significant effect on the oxygen surface mobility and among the different metals (Rh, Pt, Pd, Ru) Rh is the most active. It is suggested [37] that the greater activity of Rh is due to its p-semiconductor nature, with a highly population of oxygen species loosely bonded to the surface. In another work [36,38], it was found that the energy of exothermic process of N_2O decomposition ($\Delta H = -19.5$ kcal mol^{-1}) over Rh can be transferred to adjacent surface oxygen-adsorbed atoms allowing subsequent recombination and so called „reaction - assisted desorption" of O_2 at significantly lower temperatures.

The improved Rh metal dispersion compared to Pt suggests that this likely enhances the NO_x desorption process. However, it should be mentioned that the NO_x desorption process occurs at significantly lower temperature for Rh containing samples. Therefore, it is not likely that the increased dispersion is the only reason for this behavior. We suggest that Rh can have a significant promoting effect on the spill-over process of NO_x. This suggestion is based on the kinetic modeling and experimental data previously discussed in the literature [14,15,18,39–41], indicating that the rate limiting factor controlling the mobility of surface species between the storage sites and Pt particles on $Pt/Ba/Al_2O_3$ catalysts is the removal of oxygen from the Pt active sites. It was pointed out that the high coverage of oxygen on Pt hinders the spill-over process of NO_x to the precious metal and the subsequent desorption of NO_x [18].

3.3. NO_2 uptake and TPD

3.3.1. NO_x storage capacity and NO_x thermal stability in the absence of BaO

In Fig. 4 the evolution of the NO, NO_2 and total NO_x ($NO + NO_2$) concentrations as function of the time (A) during NO_2 uptake and as function of the temperature during TPD (B) over pure γ-Al_2O_3, Pt/Al and Rh/Al catalysts is presented. The outlet NO_x concentration profiles during storage and desorption, in the presence of CO_2 or H_2O are also displayed (Fig. 4C and D and Fig. 4E and F, respectively). In the first set of experiments presented in Fig. 4A, the NO_x

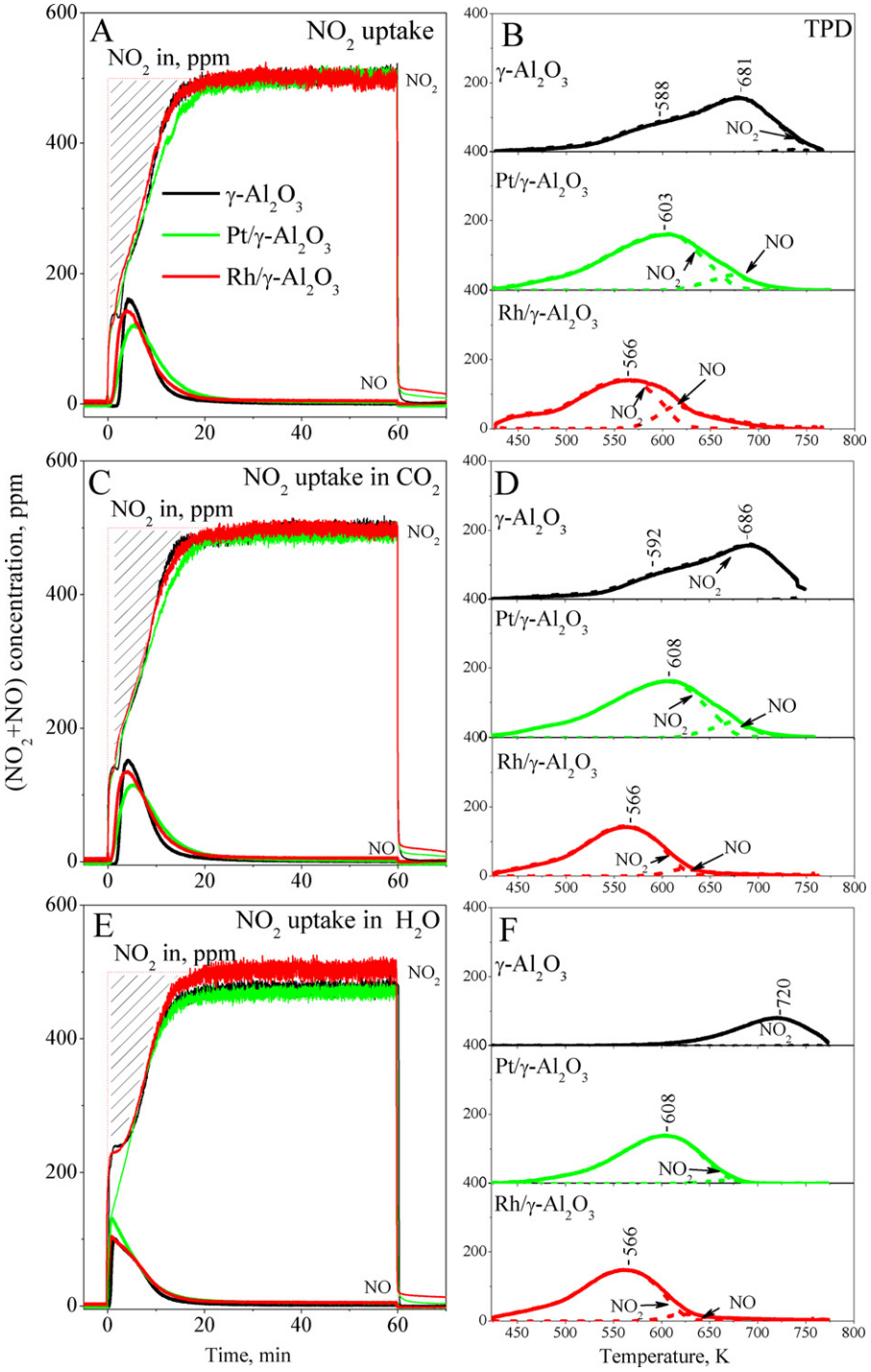

Fig. 4. Evolution of the total NO_x ($NO + NO_2$) concentration as function of the time (A) during NO_2 uptake without and in the presence of 5% CO_2 (C) or 5% H_2O (E) and as function of the temperature during TPD (B, D and F) over γ-Al_2O_3, Pt/Al and Rh/Al. The catalysts were exposed to 500 ppm NO_2 for 1 h and after flushing with Ar for 30 min, the temperature was raised to 773 K with a ramp speed of 10 K min^{-1} exposed at 423 K.

breakthrough (first evidence of NO_x in the outlet gas) was detected immediately when the NO_2 exposure is initiated, with the exit NO_2 concentration steadily increasing with time approaching the inlet NO_2 concentration level of 500 ppm (dotted line). Moreover, after the NO_x breakthrough, the evolution of NO is also observed (approximately starting from 90 s for γ-Al_2O_3 and 10 s for Pt/Al and Rh/Al). At the latest stages of the adsorption where the surface saturation of the samples with NO_x is almost completely achieved, the outlet NO_x (NO_2) concentration profile reaches a steady-state level. At the end of the storage period (1 h), upon NO_2 shutoff, the rapid decrease of the NO_x concentration is observed with appearance of a tail in the profile due to the desorption of weakly adsorbed species, whose release is favored by the decrease in the NO_x partial pressure [42]. Calculation showed that the amounts of stored NO_x are similar for all catalyst samples and near 0.47–0.48 mmol/g_{cat}. In similar way, the NO_2 adsorption experiments performed in the presence of CO_2 in the feed (Fig. 4C) showed similar NO_x uptake behavior without any significant deviations in the NO_x concentration profiles. On the other hand, a different situation is seen when the NO_x storage tests were performed in the presence of H_2O. It is

evident from Fig. 4E that the NO and NO_2 concentrations increase significantly faster in comparison with those observed during NO_2 storage in Ar and Ar/CO_2. This is also accompanied with the evolution of NO immediately when the NO_2 exposure is initiated. As a result, the NO_x adsorption capacity of the samples is decreased and is near 0.32 $mmol/g_{cat}$ in the case of alumina and near 0.41 – 0.42 $mmol/g_{cat}$ for the Pt- and Rh-containing samples. Hence, in contrast to CO_2, the presence of H_2O has a significant effect on the NO_x uptake behavior. The NO_x trapping efficiency in the presence or absence of CO_2/H_2O is summarized in Table 1. The values were determined as a percentage of the NO_2 fed by integrating the area included between the inlet NO_2 and the outlet NO_x concentration (the shaded area presented in the figures). From the table it can be seen that the NO_x trapping efficiency without or in the presence of CO_2 for Pt/Al and Rh/Al catalysts is very comparable with that for γ-Al_2O_3. The values varies between 7 and 8% for both Pt and Rh catalysts. On the other hand, it can be seen that the H_2O shows quantitatively very similar negative impact on the NO_x storage efficiency for both catalysts, indicating that the effect is not a function of the noble metal. In other words, the results clearly show that the type of the noble metal is not essential to the storage of NO_x on γ-Al_2O_3 surface when using NO_2, as expected. A number of former studies [43–45] showed that unlike CO_2, the presence of H_2O during NO_x uptake on γ-Al_2O_3 significantly decreases the total number of sites available for adsorption. This was explained [43] by a partial elimination of the NO_x adsorption sites on the alumina surface due to water adsorption and formation of surface hydroxyl groups.

The NO_x storage over γ-alumina has been thoroughly investigated by several research groups [43,46–50]. Accordingly, it was assumed that in the initial part of the experiment (t = 0–50 s) the adsorption process of NO_2 takes place directly without evolution of NO, leading to the formation of coordinately bonded surface species, e.g., nitro or nitrito groups. Then, it is suggested [46] that the adsorption process proceeds via disproportionation, leading to the formation of surface nitrates with NO evolution. In this case it is observed [41] that the NO_2 consumption can likewise be correlated to the NO yield by the stoichiometry of the disproportionation reaction, according to Eq. (10) that can be assessed using the integral $NO_{2,consumed}/NO_{,produced}$ ratio. Based on this, it was found [46] that the NO_2 uptake process over bare alumina produces one NO molecule for every three NO_2 molecule consumed:

$$O^{2-} + 3NO_2 \rightarrow 2NO_3^- + NO \uparrow \quad (10)$$

As a matter of fact, the $NO_{,produced}/NO_{2,\ consumed}$ integral ratio estimated in the case of γ-alumina is very close to the theoretical value given by Eq. (10), i.e. 0.34 vs. 0.33. Similarly to bare alumina, the NO_2 storage on Pt/Al and Rh/Al (Fig. 4A, C and E) is also accompanied by the evolution of NO, and similar integral $NO_{,produced}/NO_{2,consumed}$ ratios were estimated (0.37 and 0.34 for Pt/Al and Rh/Al, respectively). Thus, it can be argued that the NO_2 disproportionation reaction is able also to describe almost completely the NO_2 uptake process over Pt/Al and Rh/Al surfaces as well. Similar conclusions can be derived when the NO_2 storage is carried out over the investigated samples in the presence of CO_2 and water as well.

Despite the observed similarities regarding the NO_x storage behavior, Fig. 4B, D and F corresponding to the TPD analysis clearly indicates important differences among the samples related to the stabilities of the NO_x adsorbed species. It is readily visible that under all atmospheres the presence of the noble Pt or Rh metals on the support surface has considerable effect on the NO_x release which occurs at lower temperatures in comparison with that of γ-Al_2O_3. Moreover, this effect is more noticeable on Rh/Al catalyst with respect to that of Pt/Al system. This indicates that Pt and Rh appear to have an impact on the thermal stabilities of the trapped NO_x which do not depend on the presence or absence of CO_2 or H_2O in the feed gas during desorption process.

In terms of the general trends observed in Fig. 4B, D and F, it can be seen that the total NO_x concentration profile corresponding to γ-Al_2O_3 contains a broad desorption feature with maximum at 681 K and a shoulder at relatively lower temperature region. In the light of the numerous former studies [43,47–50] focused on FTIR and TPD experiments upon NO_2 adsorption on the γ-Al_2O_3, the main desorption peak with the shoulder observed in the TPD were attributed to decomposition of bridging and bidentate nitrates [43,47–50], yielding predominantly NO_2. The presence of Pt or Rh to the support surface brings about a visible change in the NO_x desorption profile: in contrast to γ-Al_2O_3, the TPD of the noble metal containing samples present a strong asymmetric NO_x desorption peak with maxima shifted in the lower temperature region at 603 K and 566 K for Pt/Al and Rh/Al, respectively. Moreover, for both catalysts, the initial stages of desorption process are accompanied with the evolution of significant amount of NO_2 while those at relatively high temperatures are related to NO_x release with partial noble metal-catalyzed NO_2 decomposition to form small amounts of NO.

3.3.2. NO_x storage capacity and thermal stability in the presence of BaO

Fig. 5 illustrates the NO_x uptake behavior and the thermal stability of the NO_x adsorbed species formed on the surface of both ternary Pt/Ba/Al and Rh/Ba/Al systems. The results corresponding to the binary Ba/Al system used as a reference sample are also presented. In the case of the experiments carried out under Ar and Ar/CO_2 (Fig. 5A and C), upon NO_2 exposure the outlet NO_2 concentration increased rapidly and then switched over to a gradually increase to approach the inlet concentration (dotted red line). In the meantime NO was also detected. A different situation is observed in the presence of H_2O (Fig. 5E), since in this case the approach to the inlet concentration is much slower and at the end of the adsorption procedure (1 h) the outlet NO_2 concentration has not yet reached the inlet concentration value. Moreover, from Fig. 5A, C and E, it is evident that the behavior of the ternary Pt/Ba/Al and Rh/Ba/Al catalysts follows that of the reference Ba/Al sample, i.e. the NO_2 adsorption is dominated by the Ba/Al components. In fact apparently the presence of different noble metals has no significant effect on the breakthrough profiles and on the corresponding NO_2 uptake behavior of the ternary Pt/Ba/Al and Rh/Ba/Al systems. This can be also clearly seen from the corresponding NO_x trapping efficiency in the presence or absence of CO_2/H_2O, presented in Table 1. The NO_x trapping efficiency values measured without and in the presence of CO_2 are very comparable for all samples and vary in the range of about 13.5–14.4%. On the contrary, the amount of NO_x stored is more significant in the presence of 5% H_2O for all samples presented in Fig. 5E: the NO_x trapping efficiency is roughly doubled in the presence of H_2O and is near 25–27%. It is obvious that the NO_x storage on BaO-based catalysts is not a function of the noble metal when using NO_2. The results clearly show that the NO_x storage on the BaO component (or on the $BaCO_3$ component in the presence of CO_2, as under actual conditions) into the ternary catalytic systems could also be described through the dispropotionation mechanism [18,41,46].

$$BaO/(BaCO_3) + 3NO_2 \rightarrow Ba(NO_3)_2 + NO \uparrow + (CO_2) \uparrow \quad (11)$$

As a matter fact, in the adsorption runs carried out in Ar and Ar/CO_2 the $NO_{,produced}/NO_{2,consumed}$ integral ratio is very close to the theoretical value given by Eq. (11), i.e. in the range 0.34–0.36 vs. 0.33. In addition, it is also apparent that the presence of H_2O increases the amounts of NO_x stored on the surface. Previous literature data [51] showed that the presence of H_2O induces significant phase transformations of pre-adsorbed NO_2 into bulk crystalline

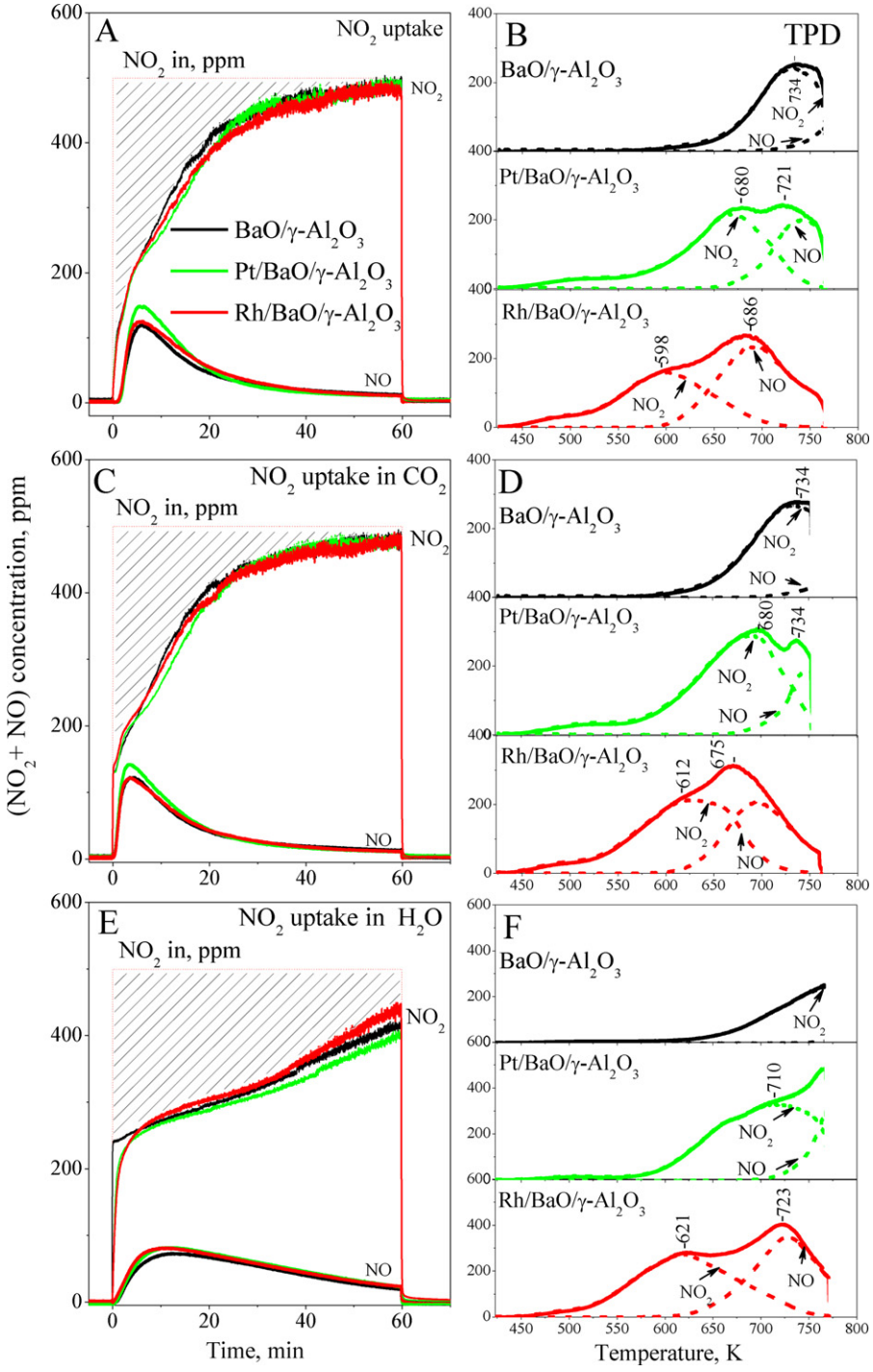

Fig. 5. Evolution of the total NO_x ($NO + NO_2$) concentration as function of the time (A) during NO_2 uptake without and in the presence of 5% CO_2 (C) or 5% H_2O (E) and as function of the temperature during TPD (B, D and F) over Ba/Al, Pt/Ba/Al and Rh/Ba/Al. The catalysts were exposed to 500 ppm NO_2 for 1 h and after flushing with Ar for 30 min, the temperature was raised to 773 K with a ramp speed of 10 K min^{-1} exposed at 423 K.

$Ba(NO_3)_2$ particles on the surface. Thus, the corresponding slower rate of NO_x adsorption, observed in Fig. 5 (E) could be explain by the formation of such bulk-like $Ba(NO_3)_2$ particles in the initial period of the NO_2 exposure in 5% H_2O which exhibit less accessible surface sites for fast NO_x saturation. This explanation is also in good agreement with the observed NO_x breakthrough profiles, which did not achieve a steady-state. In other words, the decreased rate of NO_x uptake in the presence of H_2O which is observed initially during the storage can probably be attributed to the diffusion limitations through the formed bulk crystalline $Ba(NO_3)_2$ particles on the surface which hinders the storage process to the available Ba trapping sites. On the other hand, the formation of bulk-like particles may also be a contributing factor for the improved NO_x trapping efficiency in H_2O [52]. A comparative analysis of TPD profiles in Fig. 5B, D and F clearly shows more significant differences between the samples related to the relative surface stabilities of NO_x adsorbed species. For elucidation of the effect of the precious metals on the thermal behavior of the ternary Pt/Ba/Al and Rh/Ba/Al catalysts the results should be referred to the TPD data given for Ba/Al reference sample. It can be seen that the broad

desorption NO_x concentration profile observed for Ba/Al (Fig. 5B) can be derived into two desorption regions. The decomposition process resulted in the initial evolution of significant amounts of NO_2 with maximum at 734 K, followed by minor NO released in the higher-temperature region of the NO_x profile. In agreement with the numerous studies in the literature [43,48–56] focused on the NO_x-TPD of the BaO/γ-Al_2O_3 system, the major NO_2 feature can be assigned to the decomposition of surface nitrates associated with the BaO monomers/dimers strongly interacting with the support. The evolution of small amounts of NO at higher temperatures was on the other hand related to the decomposition of bulk nitrates which are relatively more stable than the surface nitrates, and which decomposition yields mostly NO and O_2 [43,48–51].

The analysis of the TPD data in Fig. 5B corresponding to the Pt or Rh-based Ba/Al catalysts reveals analogous trend in the evolution of NO_x ($NO + NO_2$) in the course of the desorption process, similar to that of the Ba/Al sample while heating in Ar. However, both NO_2/NO signals are significantly shifted toward lower desorption regions with increasing the temperature. Moreover, the effect is much more strongly pronounced in the TPD profile of the ternary catalytic systems with Rh in comparison with that of Pt/Ba/Al. NO_2 was detected to desorb in a single asymmetric peak with a maximum at 680 K and 598 K for Pt/Ba/Al and Rh/Ba/Al catalysts, respectively. The NO desorption profiles contain a broad desorption peak with an initial maximum at 721 K and 686 K for Pt/Ba/Al and Rh/Ba/Al and then tailed off toward higher temperatures. It should be noted that such thermal destabilization of the NO_x adsorbed species when Pt and especially Rh was present, was also observed when CO_2 or H_2O was introduced individually during the desorption process (Fig. 5D and F).

The thermal destabilization effect of Pt in the decomposition temperature of stored nitrates is well established in numerous studies in the literature [4,18,56,57], suggesting that the decomposition of nitrates occurs at the interface between the Ba component and the noble metal, which thus promotes nitrate decomposition. Notably, a detailed modeling study of NO_x storage and TPD [41] showed that the higher temperature of NO_x desorption on Pt-free BaO/Al_2O_3 system can be also explained by re-adsorption process, since NO_2 liberated upon barium nitrate decompositions may re-adsorbs on free BaO sites when they are created downstream and subsequently decomposes at a higher temperatures. However, this is not the case at lower temperatures, since the main part of the NO_x desorbed at lower temperatures is in the form of NO_2 to NO and O_2 also over the noble metal containing samples. This is well described by Olsson et al. [18] in a kinetic model of the overall process of NSR performance on $Pt/BaO/\gamma$-Al_2O_3 monolith catalysts: the model successfully describes the observed lower thermal stability of stored NO_x during TPD when Pt was present by invoking a mechanism for the release of NO_x including spill-over of NO_x to Pt and subsequent desorption of NO_x from noble metals sites. In addition, it is concluded that the higher mobility of the surface species between the storage sites and Pt particles can be significantly limited at high coverage of oxygen on Pt. In the kinetic model developed by Olsson et al. [18] is suggested that the rate limiting step of NO_x release is the oxygen desorption from the noble metal sites, which is in very good agreement with our experimental results discussed above. Thus, it can be argued that the presence of Rh on the catalytic surface promotes the NO_x desorption process at lower temperatures than Pt, which we also observe experimentally. The lowered temperature of O_2 release from the surface of Rh catalysts could leave a significant number of noble metal sites accessible for adsorption. Thus, this could facilitate the rate of spill-over of NO_x from the storage site (the surface sites on γ-Al_2O_3 and those on BaO) to the noble metal and the subsequent desorption of NO_x at lower temperatures. Along these lines, it can also be proposed that the rate limiting aspects related to the spill-over of NO_x on the surface under rich conditions during the NSR operation are much more suppressed when the noble metal is present in the catalysts with higher regeneration ability. The promoting effect of Rh catalysts on the rate of the kinetic process of transport of NO_x through the surface can be explained by envisioning a location of the available noble metal sites well dispersed on the surface, which provides an additional Rh/Al_2O_3 interface for spill-over to occur.

Another important aspect regarding the thermal behavior of the studied samples is the difference between the product distributions of NO_2 and NO originating from the decomposition of the stored NO_x in the presence of the noble metals (Fig. 5B, D and F). This has been described in the literature [57] due to noble metal-catalyzed NO_2 decomposition. Along these lines, comparison of the TPD profiles (Fig. 5B and D) reveals that the intensity ratio of NO to NO_2 is greater for Rh/Ba/Al catalyst than that for Pt/Ba/Al, suggesting for stronger promotional effect of Rh on the NO_2 decomposition reaction leading to NO formation. It should be noted however, that this effect is notably suppressed in the presence of 5% CO_2 fed during desorption process.

3.4. Storage and reduction cycling on Pt/Al and Rh/Al

The NSR performance of the Pt/Al and Rh/Al catalysts were tested in the temperature range of 473–673 K over the course of 10 lean/rich cycles. In Fig. 6 two consecutive storage and reduction cycles at different reaction temperatures 473, 573 and 673 K are presented, after the system had reached a cyclic steady-state for Pt/Al (Fig. 6A, B and C) and Rh/Al (Fig. 6D, E and F) catalysts. The evolution of total NO_x and NO along with the product distribution of NO_2, NH_3, N_2O and CO in the outlet stream as a function of the time is plotted. In addition, the amounts of stored NO_x species during the lean phase, the NO conversion, the NO_x trapping/removal efficiency, the product selectivity to N_2/NH_3 were calculated by Eqs. (2)–(8) and the results are reported in Fig. 7 and 8, respectively. Concerning the results given in Fig. 6, both catalysts exhibit typical profiles consistent with the NSR operation similar to that reported in the literature [24,58]. Accordingly, upon NO admission to the lean phase, NO_x ($NO + NO_2$) breakthrough immediately appeared, with the exit total NO_x concentration steadily increasing with time, approaching the inlet NO concentration level of 500 ppm (black line). It can be seen that the NO_2 product distribution and the amounts of NO_x stored on the surface at this point (the shaded area included between the inlet NO and the outlet NO_x concentration in Fig. 6A) vary depending on the reaction temperature and on the sample composition (see Figs. 7 and 8). Comparison of the results in Fig. 6 reveals that Pt/Al catalyst exhibited superior NO_x storage capacity at 473 and 573 K than that of Rh/Al. This can also clearly be seen from Fig. 7 which shows the calculated total NO_x stored as function of the reaction temperature. The amounts of stored NO_x on Pt/Al at 473 and 573 K were 6.42×10^{-2} and 5.14×10^{-2} mmol/g_{cat}, while the values estimated for Rh/Al are significantly lower at the same temperatures 1.78×10^{-3} and 7.74×10^{-3} mmol/g_{cat}. A further increase in the reaction temperature to 673 K, leads to a considerable decrease of storage capacity for both Pt/Al and Rh/Al catalysts and calculated amounts of NO_x stored were 1.33×10^{-2} and 1.43×10^{-2} mmol/g_{cat}, respectively.

It is well known [59] that the changes in the NO_x breakthrough profiles is a function of the relative rates of NO oxidation on the noble metal sites, the NO_x diffusion to the storage surface sites and the NO_x trapping ability. Indeed, the observed different NO_x trapping efficiency of Pt/Al and Rh/Al catalysts during the lean period (Fig. 8B) can be correlated to the different NO oxidation and storage ability (Fig. 8A). During the lean cycles, the NO oxidation seems to be operating over Pt/Al catalysts at 473 K. The overall NO conversion to 29.3% at 473 K has resulted in relatively low NO_x trapping efficiency (about 15%). In contrast, no substantial NO oxidation was

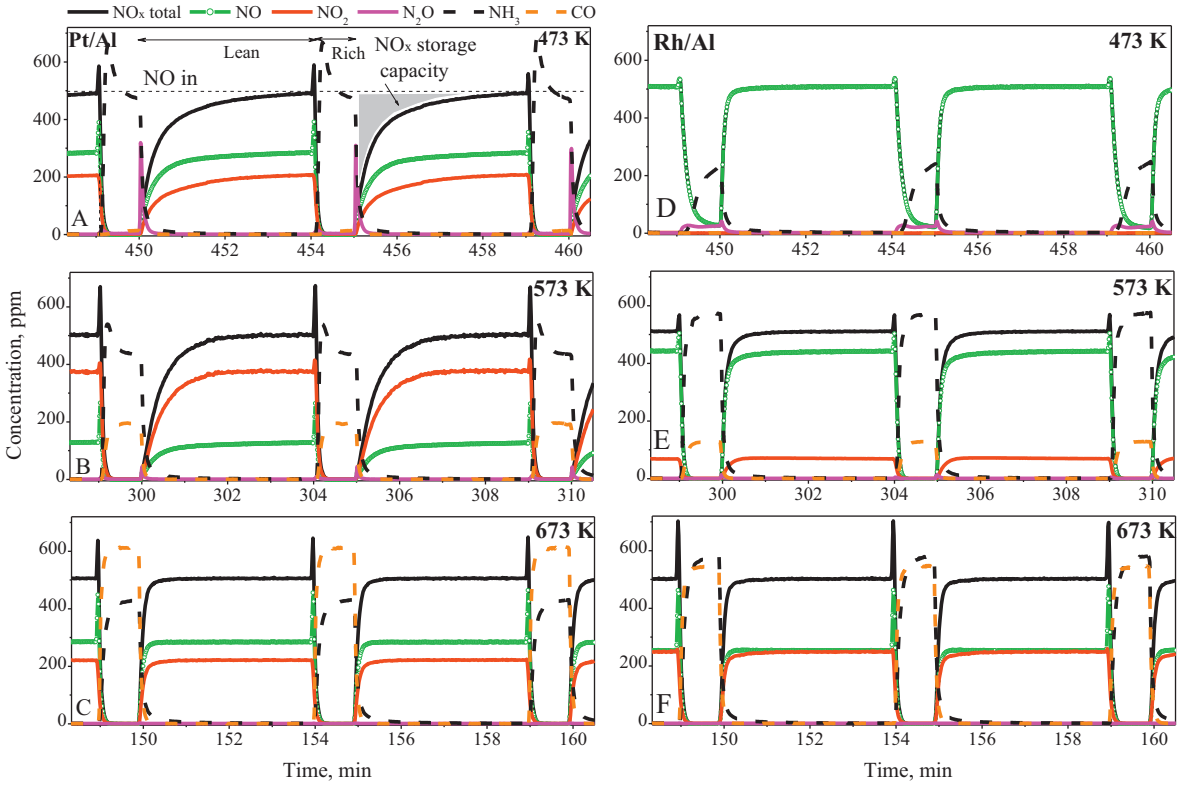

Fig. 6. Evolution of total NO_x, NO, NO_2, N_2O, NH_3 and CO of the outlet gas composition during two alternative lean/rich cycles in 500 ppm NO, 10% O_2 (or 1% H_2), 5% H_2O and 5% CO_2 at different temperatures (473, 573 and 673 K) for Pt/Al (A, B and C) and Rh/Al (D, E and F) catalysts.

observed over Rh/Al catalysts at 473 K (Fig. 6D). Furthermore, the produced NO_2 over Pt/Al system reaches the highest concentration (about 375 ppm) at 573 K where a maximum NO conversion (42.9%) is achieved (Figs. 7B and 9). However, despite the observed maximum in the NO conversion, Pt/Al catalyst exhibited lower NO_x trapping ability at this temperature. The curve demonstrating the changes in the NO_x trapping efficiency with increasing the temperature does not follow similar profile to that of the NO conversion. Moreover, this becomes more obvious with an increase the temperature up to 673 K where the NO_x trapping efficiency is negligible while the Pt/Al catalyst is still able to keep some NO oxidation and NO conversion (30.8%). Similar alterations can also be seen for Rh/Al catalyst where the NO_x trapping efficiency is negligible in the entire range of the examined temperatures. The reason for this is lowered thermal stability of the NO_x species adsorbed on the alumina surface which was observed for both Pt/Al and Rh/Al catalysts (see Fig. 4 (F)), hindering the ability of the alumina sites toward gas phase NO_x adsorption at higher temperatures.

It can readily be seen that the NO oxidation conversion curve for Pt/Al is characterized with a maximum at about 573 K. This result is in agreement with former studies [60,61] in the literature, indicating that the decrease of NO conversion at higher temperatures

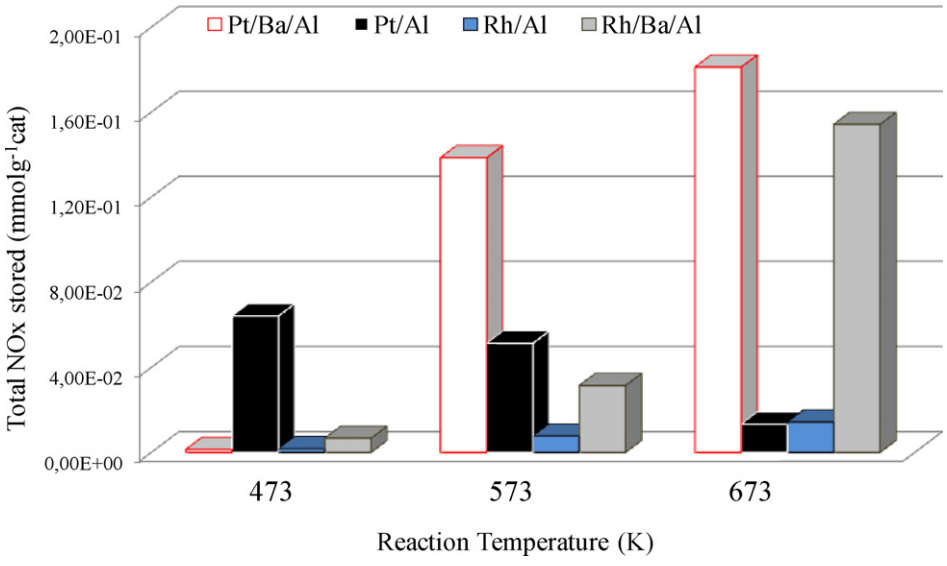

Fig. 7. Estimated amounts of stored NO_x species during the lean phase on the Pt- and Rh-containing catalysts as function of the reaction temperature.

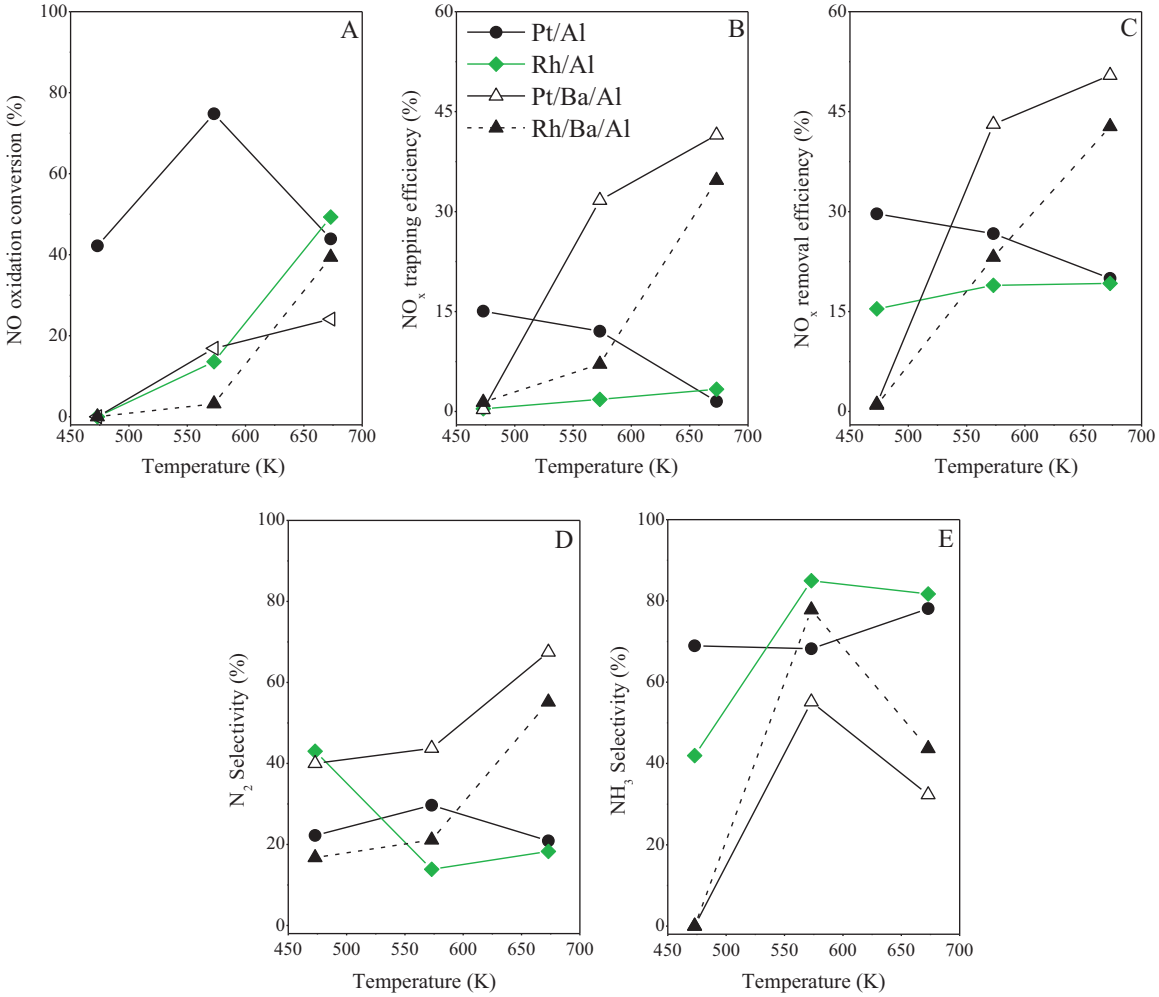

Fig. 8. NO oxidation conversion (A), NO_x trapping/removal efficiency (B/C) and selectivity to N_2 (D) and NH_3 (E) as function of the reaction temperature over Pt/Al, Pt/Ba/Al, Rh/Al and Rh/Ba/Al catalysts.

above 573 K is a result of the shift to an equilibrium-limited regime. In addition, it was also reported that Pt is a good oxidation catalysts and can rapidly convert NO to NO_2, which is subsequently stored predominantly as nitrates [6].

Such a situation is not valid for the monometallic Rh/Al catalyst where the reaction occurred by negligible NO oxidation conversion as indicated by the low level of NO_2 exiting the reactor at 473 and 573 K. The very low NO_x trapping efficiency in this case of Rh-containing system strongly suggests that the rate of NO_x storage is likely to be limited from the low NO oxidation performance of the Rh catalyst. The results are in agreement with the former [10] investigations, revealing the poor performance of Rh catalysts in storing of NO_x.

During the switch to rich conditions (Fig. 6), at the initial phase of the reduction period a sharp spike in the NO concentration can be seen for both catalysts, indicating that some NO_x may leave the reactor unconverted. This was attributed [24,58] to the lowered stability of the stored NO_x species when decreasing the oxygen partial pressure. In fact the extent of the NO puff is related to the amounts of NO_x stored onto the catalysts. It is apparent that the NO_x stored during the lean period reacted with the inlet H_2 after the switch to rich conditions and the overall reduction is resulted mainly to production of NH_3 and CO accompanied with the formation of small quantities of N_2O. N_2 is also formed, as confirmed by the N-balance (see below), although its presence is not detected by the FTIR analyser. Representative results showing the NO_x removal efficiency and the product selectivity to N_2 and NH_3 are presented in Fig. 8C, D and E, respectively. The selectivity trends, presented in Fig. 8D and E showed that the product distribution of N_2 and NH_3 strongly varies depending on the reaction temperature and on the sample composition. Generally, most of the change in the N_2 selectivity was reflected as an opposite change in the NH_3 selectivity. The increase in N_2 selectivity with temperature to 573 K comes at the expense of NH_3 selectivity which achieved its highest values (78.1%) at 673 K. NH_3 formation originates from reaction of gas-phase NO with H_2 (500 ppm NO are present during the rich phase):

$$NO + 5/2H_2 \rightarrow NH_3 + H_2O \quad (12)$$

Due to the high H_2/NO feed ratio in the gas phase, high NH_3 selectivity is expected. However, the unselective reduction of the stored NO_x also contributes to NH_3 formation, as discussed elsewhere [62,63]. For Rh/Al sample, N_2 was the favored product at the lowest temperature than that of Pt/Al, approaching 21.5% at 473 K. This result is consistent with the observations in the literature [64], which shows that Rh is more effective than Pt in converting NO to N_2 rather than NH_3 under steady–state conditions, although the difference diminished with aging the catalyst.

Over Pt/Al, nitrous oxide formation is also observed, with a peak in correspondence of the rich/lean switch. Its formation decreases with temperature and at 673 K the production of N_2O is negligible. As discussed elsewhere [64], it is likely that N_2O formation involves the reaction of NH_3 with NO in the presence of oxygen, i.e.

conditions which are met upon oxygen admission in the lean phase. Its formation decreases with temperature being decomposed to N_2 and O_2 over Pt [65]. The results in Fig. 8C reveal that the limited performance of Rh in the NO oxidation was translated not only to the lowered NO_x storage but also to a decrease in the NO_x removal efficiency in comparison to the corresponding monometallic Pt/Al sample over the temperature range of 473–573 K. In general terms, it is evident that Pt/Al catalyst shows similar trend of progressive decrease of NO_x removal efficiency with increasing the temperature which as discussed before is due to mainly to the analogous trend of the continuous decrease of NO_x stored species over alumina surface. The maximum NO_x conversion for Pt/Al was 29.6% at 473 K.

Finally, CO is also produced over both catalysts from the reverse water gas shift reaction (RWGSR) between CO_2 and H_2 (Eq. (13))

$$CO_2 + H_2 \leftrightarrow CO + H_2O \quad (13)$$

producing H_2O along with CO. Pt- and Rh-based catalysts show similar activity in this reaction as pointed out by the comparable CO concentration levels observed during the rich phase.

3.5. Storage and reduction cycling on Pt/Ba/Al and Rh/Ba/Al

Further insight regarding the influence of the presence of BaO NO_x storage component on the NSR performance of Pt and Rh catalysts was obtained by activity measurements conducted under identical cycling operation conditions with both Pt/Ba/Al and Rh/Ba/Al catalysts. The evolution of NO_x, NO, NO_2, NH_3, N_2O and CO with time after the Pt/Ba/Al and Rh/Ba/Al systems had reached a cyclic steady-state are presented in Fig. 9 for two consecutive storage and reduction cycles at different reaction temperatures (473–673 K). Similarly to the non-Ba-containing catalysts, Figs. 7 and 8 show the main parameters, which were used to describe the overall NSR performance of the ternary systems. The analysis of the results for both ternary Pt/Ba/Al and Rh/Ba/Al catalytic systems presents notable dissimilarities in the whole temperature range to the data given in Figs. 6–8, summarizing the results of the cycling experiments performed on the Pt/Al and Rh/Al catalysts without Ba. The results obtained at 573 and 673 K (Fig. 9B, C, E and F), during the lean cycles, indicated higher activity for NO_x storage of both Pt/Ba/Al and Rh/Ba/Al in comparison to the corresponding binary systems. Barium promotes the storage process leading to maximum NO_x storage capacity at 673 K for both catalysts. This expected increase in the amount of stored NO_x at higher temperatures with respect to the corresponding non-Ba-containing Pt/Al and Rh/Al catalysts (Fig. 7) can be attributed to the higher thermal stability of NO_x adsorbed species on BaO sites than that of those stored on bare alumina as pointed out above and in line with literature [48–50].

Comparison of the data in Figs. 7 and 8B, indicates lower NO_x storage capacity and lower NO_x trapping efficiency in the range of 573–673 K again for Rh/Ba/Al catalyst with respect to the Pt/Ba/Al system. The amounts of stored NO_x on Pt/Ba/Al at 573 and 673 K were 1.39×10^{-1} and 1.81×10^{-1} mmolg^{-1} catalyst corresponding to a NO_x trapping efficiency at the same temperatures of 31.7% and 41.5%, respectively. The Rh/Ba/Al catalyst is characterized with significantly lower NO_x storage capacity since the calculated amounts of NO_x stored were 3.15×10^{-2} at 573 K and 1.54×10^{-1} mmolg^{-1} catalyst at 673 K (corresponding to NO_x trapping efficiency for Rh/Ba/Al near 7.1% at 573 K and 34.7% at 673 K). Again, the possible explanation to this effect was the limited role of Rh in comparison with Pt to the rate-controlling process of NO oxidation to NO_2 during storage.

Along these lines, the dependence of the NO oxidation conversion over the temperatures examined in Fig. 8A, reveals that the outlet NO_2 in the course of the lean periods over Pt/Ba/Al system reaches the highest concentration (about 100 ppm) at 673 K where a maximum NO conversion (24.1%) is achieved. However, higher activity for NO oxidation at 673 K is observed with the Rh/Ba/Al catalyst. This is also seen, from Fig. 9F, by the much larger generation of NO_2 exiting the reactor at 673 K. It is possible that due to the higher NO_x storage on the Pt/Ba/Al compared with the Rh/Ba/Al, larger amounts of NO_2 are consumed, leaving lower concentration of NO_2 into the outlet stream. Further, the addition of barium to Pt/Al significantly decreases the activity for NO oxidation, which has been observed previously [6,16]. There are several possible reasons for this, one being that some Ba domains are located on the noble metal (Pt or Rh) crystallites, effectively blocking the access of the active precious metal sites to NO oxidation. Indeed, the dispersion of Pt and Rh is significantly lower after addition of barium (see Table 1). Another possibility is that since barium is alkaline platinum in Pt/Ba/Al will more easily form Pt oxide [6], which is suggested to have a lower activity for NO oxidation [66]. The lower NO_x trapping efficiency for Rh/Ba/Al compared to Pt- based catalyst at temperatures in the range of 573–673 K translates to a corresponding reduction in the NO_x conversion. This can readily be seen in Fig. 8C, where the Pt/Ba/Al system is characterized with a maximum in the NO_x removal efficiency, approaching 50.4% at 673 K while the value estimated at the same temperature for Rh/Ba/Al was 42.7%. Another important aspect regarding the catalytic behavior of the studied samples is the difference between the N_2 and NH_3 product distributions with increasing the temperature (Fig. 8D and E). The NO_x reduction process occurred for both catalysts at 573 K directly through the predominant formation of NH_3 at the expense of N_2. A further increase in the reaction temperature to 673 K, leads to a considerable decrease of the NH_3/N_2 yield ratio however, the calculated N_2 selectivity remains higher for Pt/Ba/Al catalyst (33.7%) with respect to Rh/Ba/Al (27.6%) sample. In a agreement with the literature data [7,67,68], the decreased NH_3 formation with increasing temperature to 673 K has been related partially as a result of the lower nitrite/nitrate species stability, such that the released NO_x: reductant ratio is too high for substantial NH_3 formation. In addition, it was previously found [68] that the fraction of NO_x that is reduced to NH_3 is much more at lower temperatures when more NO_x species are available over a longer period of time due to the slower diffusion rates between the storage sites and Pt.

The cycling data reported so far involved the evolution of the main parameters, which described the overall NSR performance of the ternary systems in the temperature range of 573–673 K. On the other hand, a decrease of the reaction temperature to 473 K was able to provide additional information. The results in Fig. 9A and D clearly show the detrimental effect of the low temperature (473 K) on the overall NSR performance of both catalysts. During the lean cycles, no substantial storage was observed without the appearance of any NO_2 as a product of oxidation reaction. During the switch to rich conditions, the NO_x conversion was minimal over both samples, suggesting that the NSR performance is not operating at this temperature. A more detailed comparison of the results during the whole period of lean and rich cycles performed at 473 K with the Pt/Ba/A and Rh/Ba/Al catalysts is presented in Fig. 10A and B. Lowering the reaction temperature produced significant differences in the first few cycles for Pt/Ba/Al samples as can be seen in Fig. 10A. The start of the first three cycles during the lean phase coincided with the evolution of small amounts of NO_2, immediately when the NO exposure is initiated, with the exit concentration steadily increasing with time, approaching concentration level of about 45 ppm. Apparently, the NO oxidation seems to be operating over the Pt/Ba/Al catalyst in the first few cycles. Concerning the reduction periods in these three cycles, however, clearly indicated a gradual decrease of NO_x conversion from one cycle to the next, until the regeneration ability was completely lost after the third

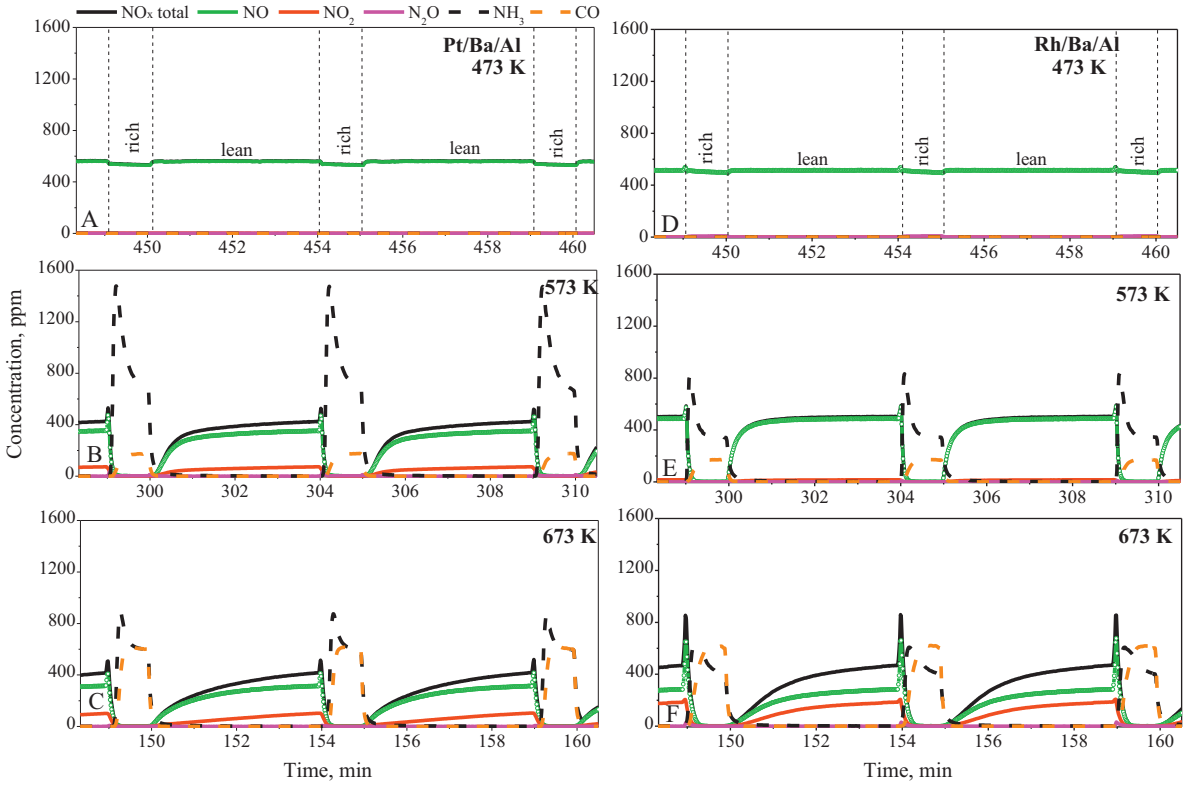

Fig. 9. Evolution of total NO_x, NO, NO_2, N_2O, NH_3 and CO of the outlet gas composition during two alternative lean/rich cycles in 500 ppm NO, 10% O_2 (or 1% H_2), 5% H_2O and 5% CO_2 at different temperatures (473, 573 and 673 K) for Pt/Ba/Al (A, B and C) and Rh/Ba/Al (D, E and F) catalysts.

cycle. This behavior was previously reported by Breen et al. [8] for Pt catalysts and it was explained by the gradual deterioration of the surface from cycle to cycle until an equilibrium point between the rates of reduction and storage is reached. Such a situation is not valid for the Rh/Ba/Al (Fig. 10B), where there was no significant NO_x storage during the whole cycling experiment, due the poor NO oxidation ability. This is evident from all lean cycles where no NO_2 was detected. Further, also no NO_x reduction was observed at 473 K in the rich period over Rh/Ba/Al.

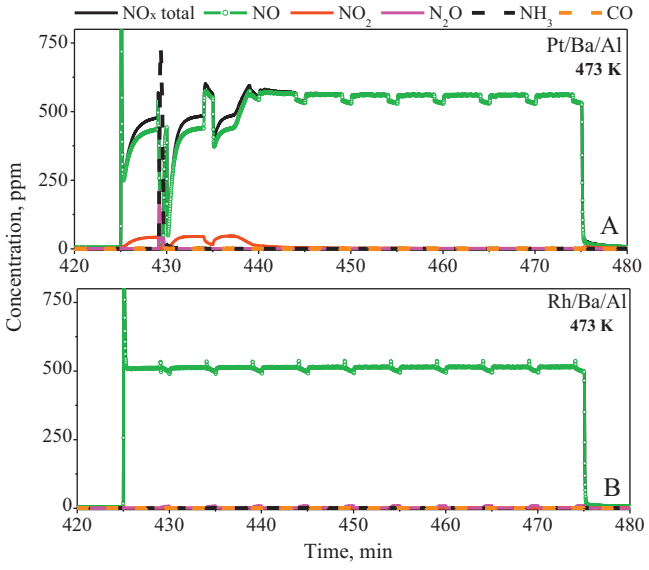

Fig. 10. Evolution of total NO_x, NO, NO_2, N_2O, NH_3 and CO of the outlet gas composition during 10 alternative lean/rich cycles in 500 ppm NO, 10% O_2 (or 1% H_2), 5% H_2O and 5% CO_2 at 473 K for Pt/Ba/Al (A) and Rh/Ba/Al (B) catalysts.

4. Conclusions

In the light of the results reported in the current work, the main conclusions can be summarized as follows:

(a) It was found that the Rh/Al and Rh/Ba/Al catalysts are more active than the corresponding Pt catalysts in the catalytic N_2O decomposition reaction due to the „reaction - assisted" release of O_2 at significantly lower temperatures. Hence, the Rh addition as precious metal to the conventional NO_x storage $Ba/\gamma\text{-}Al_2O_3$ based catalysts provides superior ability compared to Pt to accelerate the O_2 release from the catalytic surface at lower temperatures, maintaining Rh in metallic state.

(b) Due to the improved Rh metal dispersion and the ability of Rh catalysts to release O_2 from the surface at lower temperatures with respect to that of Pt, it is suggested the existence of a significant promoting effect on the spill-over process of NO_x to the precious metal, controlling the subsequent desorption of NO_x. The results clearly showed that the addition of the precious Rh metal into the $BaO/\gamma\text{-}Al_2O_3$ system has a considerable effect on the metal support interaction, by assisting the desorption of nitrate species at a significantly lower temperature in comparison with that of the Pt-containing catalysts. The lowered thermal stability of the NO_x adsorbed species when Rh is present was also evident when CO_2 or H_2O was introduced individually during the desorption process.

The lowered temperature of O_2 release from the surface of Rh catalysts may leave a significant number of noble metal sites available for adsorption and thus this could facilitate the rate of spill-over of NO_x from the storage site (the surface sites on $\gamma\text{-}Al_2O_3$ and those on BaO) to the noble metal and their desorption at lower temperatures. This can explain the desorption of NO_x at lower temperatures for the Ba- containing samples. On the

other hand, the promoting effect of the Rh catalysts on the rate of the kinetic process of transport of NO_x through the surface was explained by envisioning a location of the available noble metal sites well dispersed on the surface, which provides an additional Rh/Al_2O_3 interface for spill-over to occur.

(c) The presence of H_2O was found to have significant influence on the overall NO_x storage performance of both ternary Pt and Rh-based $Ba/\gamma\text{-}Al_2O_3$ catalysts by increasing the NO_x trapping efficiency, when using NO_2 as NO_x precursor. The increased amounts of NO_x stored on the surface were attributed to the diffusion limitations through the formed bulk-like particles.

(d) The limited NO_x storage ability of the Rh-based $BaO/\gamma\text{-}Al_2O_3$ catalysts under lean-burn conditions was found to originate from both low NO oxidation and NO_x reduction activity, while the main limiting factor for the low NSR performance of the Pt-based $BaO/\gamma\text{-}Al_2O_3$ was the limited regeneration ability of the Pt active sites during rich periods.

Acknowledgment

This work has been performed at the Competence Centre for Catalysis in collaboration with Politecnico di Milano. KCK is financially supported by Chalmers University of Technology, the Swedish Energy Agency and the member companies: AB Volvo, Volvo Car Corporation, Scania CV AB, Haldor Topsoe A/S and The Swedish Space Corporation. We would like to acknowledge the Swedish Energy Agency, Swedish Science Council, Swedish foundation for strategic research (F06-0006) and Chalmers Initiative Transport, for funding.

References

[1] J. Kabusjiki, in: Toyota (Ed.), EP658370, 1994.
[2] S.i. Matsumoto, CATTECH 4 (2000) 102-109.
[3] N. Takahashi, H. Shinjoh, T. Iijima, T. Suzuki, K. Yamazaki, K. Yokota, H. Suzuki, N. Miyoshi, S.-i. Matsumoto, T. Tanizawa, T. Tanaka, S.-s. Tateishi, K. Kasahara, Catalysis Today 27 (1996) 63–69.
[4] W.S. Epling, L.E. Campbell, A. Yezerets, N.W. Currier, J.E. Parks, Catalysis Reviews 46 (2004) 163–245.
[5] S. Roy, A. Baiker, Chemical Reviews 109 (2009) 4054–4091.
[6] L. Olsson, E. Fridell, Journal of Catalysis 210 (2002) 340–353.
[7] P. Forzatti, L. Lietti, N. Gabrielli, Applied Catalysis B: Environmental 99 (2010) 145–155.
[8] J.P. Breen, R. Burch, C. Fontaine-Gautrelet, C. Hardacre, C. Rioche, Applied Catalysis B: Environmental 81 (2008) 150–159.
[9] J.P. Breen, C. Rioche, R. Burch, C. Hardacre, F.C. Meunier, Applied Catalysis B: Environmental 72 (2007) 178–186.
[10] H. Abdulhamid, E. Fridell, M. Skoglundh, Applied Catalysis B: Environmental 62 (2006) 319–328.
[11] H. Abdulhamid, J. Dawody, E. Fridell, M. Skoglundh, Journal of Catalysis 244 (2006) 169–182.
[12] A. Amberntsson, E. Fridell, M. Skoglundh, Applied Catalysis B: Environmental 46 (2003) 429–439.
[13] R. Büchel, S.E. Pratsinis, A. Baiker, Applied Catalysis B: Environmental 113–114 (2012) 160–171.
[14] N.W. Cant, I.O.Y. Liu, M.J. Patterson, Journal of Catalysis 243 (2006) 309–317.
[15] D. James, E. Fourré, M. Ishii, M. Bowker, Applied Catalysis B: Environmental 45 (2003) 147–159.
[16] D. Bhatia, M.P. Harold, V. Balakotaiah, Catalysis Today 151 (2010) 314–329.
[17] A. Kumar, M.P. Harold, V. Balakotaiah, Industrial and Engineering Chemistry Research 49 (2010) 10334–10340.
[18] L. Olsson, H. Persson, E. Fridell, M. Skoglundh, B. Andersson, Journal of Physical Chemistry B 105 (2001) 6895–6906.
[19] R.D. Clayton, M.P. Harold, V. Balakotaiah, C.Z. Wan, Applied Catalysis B: Environmental 90 (2009) 662–676.
[20] J. Dawody, L. Eurenius, H. Abdulhamid, M. Skoglundh, E. Olsson, E. Fridell, Applied Catalysis A-General 296 (2005) 157–168.
[21] A. Holmgren, B. Andersson, Journal of Catalysis 178 (1998) 14–25.
[22] P. Lööf, B. Kasemo, S. Andersson, A. Frestad, Journal of Catalysis 130 (1991) 181–191.
[23] M.H. Kim, J.R. Ebner, R.M. Friedman, M.A. Vannice, Journal of Catalysis 204 (2001) 348–357.
[24] A. Lindholm, N.W. Currier, J. Li, A. Yezerets, L. Olsson, Journal of Catalysis 258 (2008) 273–288.
[25] B. Pereda-Ayo, D. Duraiswami, J.J. Delgado, R. López-Fonseca, J.J. Calvino, S. Bernal, J.R. González-Velasco, Applied Catalysis B: Environmental 96 (2010) 329–337.
[26] H.F.J. Van't Blik, J.B.A.D. Van Zon, T. Huizinga, J.C. Vis, D.C. Koningsberger, R. Prins, Journal of Physical Chemistry 87 (1983) 2264–2267.
[27] K. Yuzaki, T. Yarimizu, S.I. Ito, K.K. Kunimori, Catalysis Letters 47 (1997) 173–175.
[28] R. Kramer, M. Andre, Journal of Catalysis 58 (1979) 287–295.
[29] J.T. Miller, B.L. Meyers, F.S. Modica, G.S. Lane, M. Vaarkamp, D.C. Koningsberger, Journal of Catalysis 143 (1993) 395–408.
[30] M. Arai, M. Fukushima, Y. Nishiyama, Applied Surface Science 99 (1996) 145–150.
[31] K. Foger, J.R. Anderson, Applications of Surface Science 2 (1979) 335–351.
[32] E.R.S. Winter, Journal of Catalysis 15 (1969) 144–152.
[33] E.R.S. Winter, Journal of Catalysis 19 (1970) 32–40.
[34] E.R.S. Winter, Journal of Catalysis 34 (1974) 431–439.
[35] R. Burch, S.T. Daniells, J.P. Breen, P. Hu, Journal of Catalysis 224 (2004) 252–260.
[36] S.-i. Tanaka, K. Yuzaki, S.-i. Ito, H. Uetsuka, S. Kameoka, K. Kunimori, Catalysis Today 63 (2000) 413–418.
[37] C. Descorme, D. Duprez, Applied Catalysis A-General 202 (2000) 231–241.
[38] S.-i. Tanaka, K. Yuzaki, S.-i. Ito, S. Kameoka, K. Kunimori, Journal of Catalysis 200 (2001) 203–208.
[39] J.A. Anderson, B. Bachiller-Baeza, M. Fernandez-Garcia, Physical Chemistry Chemical Physics 5 (2003) 4418–4427.
[40] G. Zhou, T. Luo, R.J. Gorte, Applied Catalysis B: Environmental 64 (2006) 88–95.
[41] A. Scotti, I. Nova, E. Tronconi, L. Castoldi, L. Lietti, P. Forzatti, Industrial and Engineering Chemistry Research 43 (2004) 4522–4534.
[42] L. Castoldi, I. Nova, L. Lietti, P. Forzatti, Catalysis Today 96 (2004) 43–52.
[43] J. Szanyi, J.H. Kwak, R.J. Chimentao, C.H.F. Peden, Journal of Physical Chemistry C 111 (2007) 2661–2669.
[44] W.S. Epling, J.E. Parks, G.C. Campbell, A. Yezerets, N.W. Currier, L.E. Campbell, Catalysis Today 96 (2004) 21–30.
[45] D.S.T. Toops, W. Partridge, W. Epling, J. Parks, In Proceedings of Third Joint Meeting of U.S, Sections of Combustion Institute (2003).
[46] I. Nova, L. Castoldi, L. Lietti, E. Tronconi, P. Forzatti, F. Prinetto, G. Ghiotti, Journal of Catalysis 222 (2004) 377–388.
[47] E. Ozensoy, D. Herling, J. Szanyi, Catalysis Today 136 (2008) 46–54.
[48] S.M. Andonova, G.S. Senturk, E. Ozensoy, Journal of Physical Chemistry C 114 (2010) 17003–17016.
[49] E. Kayhan, S.M. Andonova, G.S. Senturk, C.C. Chusuei, E. Ozensoy, Journal of Physical Chemistry C 114 (2010) 357–369.
[50] G.S. Şentürk, E.I. Vovk, V.I. Zaikovskii, Z. Say, A.M. Soylu, V.I. Bukhtiyarov, E. Ozensoy, Catalysis Today 184 (2012) 54–71.
[51] D.H. Kim, J.H. Kwak, J. Szanyi, S.D. Burton, C.H.F. Peden, Applied Catalysis B: Environmental 72 (2007) 233–239.
[52] J.H. Kwak, D. Mei, C.-W. Yi, D.H. Kim, C.H.F. Peden, L.F. Allard, J. Szanyi, Journal of Catalysis 261 (2009) 17–22.
[53] J. Szanyi, J.H. Kwak, D.H. Kim, S.D. Burton, C.H.F. Peden, Journal of Physical Chemistry B 109 (2004) 27–29.
[54] J. Szanyi, J.H. Kwak, J. Hanson, C. Wang, T. Szailer, C.H.F. Peden, Journal of Physical Chemistry B 109 (2005) 7339–7344.
[55] P. Broqvist, I. Panas, E. Fridell, H. Persson, Journal of Physical Chemistry B 106 (2002) 137–145.
[56] N.W. Cant, M.J. Patterson, Catalysis Letters 85 (2003) 153–157.
[57] I. Nova, L. Lietti, L. Castoldi, E. Tronconi, P. Forzatti, Journal of Catalysis 239 (2006) 244–254.
[58] A. Lindholm, N.W. Currier, J. Dawody, A. Hidayat, J. Li, A. Yezerets, L. Olsson, Applied Catalysis B: Environmental 88 (2009) 240–248.
[59] E. Fridell, M. Skoglundh, B. Westerberg, S. Johansson, G. Smedler, Journal of Catalysis 183 (1999) 196–209.
[60] L. Olsson, B. Westerberg, H. Persson, E. Fridell, M. Skoglundh, B. Andersson, Journal of Physical Chemistry B 103 (1999) 10433–10439.
[61] R.L. Muncrief, P. Khanna, K.S. Kabin, M.P. Harold, Catalysis Today 98 (2004) 393–402.
[62] L. Cumaranatunge, S.S. Mulla, A. Yezerets, N.W. Currier, W.N. Delgass, F., H. Ribeiro, Journal of Catalysis 246 (2007) 29–34.
[63] L. Lietti, I. Nova, P. Forzatti, Journal of Catalysis 257 (2008) 270–282.
[64] L. Lietti, N. Artioli, L. Righini, L. Castoldi, P. Forzatti, Industrial and Engineering Chemistry Research 51 (2012) 7597–7605.
[65] N.W. Cant, D.C. Chambers, I.O.Y. Liu, Journal of Catalysis 278 (2011) 162–166.
[66] W. Hauptmann, M. Votsmeier, J. Gieshoff, A. Drochner, H. Vogel, Applied Catalysis B: Environmental 93 (2009) 22–29.
[67] W.S. Epling, A. Yezerets, N.W. Currier, Applied Catalysis B: Environmental 74 (2007) 117–129.
[68] I.S. Pieta, W.S. Epling, M. García-Diéguez, J.Y. Luo, M.A. Larrubia, M.C. Herrera, L.J. Alemany, Catalysis Today 175 (2011) 55–64.